Trinity University
Digital Commons @ Trinity

Physics and Astronomy Faculty Research | Physics and Astronomy Department

5-2020

Coarse-Grained MD Simulations Reveal Beta-Amyloid Fibrils of Various Sizes Bind to Interfacial Liquid-Ordered and Liquid-Disordered Regions in Phase Separated Lipid Rafts with Diverse Membrane-Bound Conformational States

S. Y. Cheng

Yiyi Cao
Trinity University, ycao@trinity.edu

Marzieh Rouzbehani
Trinity University, mrouzbeh@trinity.edu

Kwan H. Cheng
Trinity University, kcheng1@trinity.edu

Follow this and additional works at: https://digitalcommons.trinity.edu/physics_faculty

 Part of the Physics Commons

Repository Citation

Cheng, S. Y., Cao, Y., Rouzbehani, M., & Cheng, K. H. (2020). Coarse-grained MD simulations reveal beta-amyloid fibrils of various sizes bind to interfacial liquid-ordered and liquid-disordered regions in phase separated lipid rafts with diverse membrane-bound conformational states. *Biophysical Chemistry, 260*, Article 106355. http://doi.org/10.1016/j.bpc.2020.106355

This Post-Print is brought to you for free and open access by the Physics and Astronomy Department at Digital Commons @ Trinity. It has been accepted for inclusion in Physics and Astronomy Faculty Research by an authorized administrator of Digital Commons @ Trinity. For more information, please contact jcostanz@trinity.edu.

Author Manuscript

Author Manuscript

Author Manuscript

Author Manuscript

HHS Public Access

Author manuscript

Biophys Chem. Author manuscript; available in PMC 2021 May 01.

Published in final edited form as:

Biophys Chem. 2020 May ; 260: 106355. doi:10.1016/j.bpc.2020.106355.

Coarse-Grained MD Simulations Reveal Beta-Amyloid Fibrils of Various Sizes Bind to Interfacial Liquid-Ordered and Liquid-Disordered Regions in Phase Separated Lipid Rafts with Diverse Membrane-Bound Conformational States

Sara Y. Cheng[1], **Yiyi Cao**[2], **Marzieh Rouzbehani**[2], **Kwan H. Cheng**[2,3,*]

[1]Department of Physics, University of Texas at Austin

[2]Department of Neuroscience, Trinity University

[3]Department of Physics, Trinity University

Abstract

The membrane binding behaviors of beta-amyloid fibrils, dimers to pentamers, from solution to lipid raft surfaces, were investigated using coarse-grained (CG) MD simulations. Our CG rafts contain phospholipid, cholesterol (with or without tail- or headgroup modifications), and with or without asymmetrically distributed monosialotetrahexosylganglioside (GM1). All rafts exhibited liquid-ordered (Lo), liquid-disordered (Ld), and interfacial Lo/Ld (Lod) domains, with domain sizes depending on cholesterol structure. For rafts without GM1, all fibrils bound to the Lod domains. Specifically, dimer fibrils bound exclusively via the C-terminal, while larger fibrils could bind via other protein regions. Interestingly, a membrane-inserted state was detected for a trimer fibril in a raft with tail-group modified cholesterol. For rafts containing GM1, fibrils bound either to the GM1-clusters, with numerous membrane-bound conformations, or to the non-GM1-containing-Lod domains via the C-terminal. Our results indicate beta-amyloid fibrils bind to Lod

*Correspondence Author: Kwan H Cheng (kcheng1@trinity.edu).

PRESENT ADDRESS: [1] Kenneth S. Pitzer Center for Theoretical Chemistry and Department of Chemistry, University of California Berkeley, 94720, United States

PRESENT ADDRESS: [2] Department of Clinical Neuropsychology, University Medical Center Groningen, University of Groningen, Netherlands

9.Author Contribution

SYC contributed to formal analysis, software, investigation, visualization, methodology and writing - review & editing. YC contributed to conceptualization, investigation, visualization and formal analysis. MR contributed to conceptualization, investigation and methodology. KC contributed to conceptualization, formal analysis, funding acquisition, investigation, project administration, resources, software, supervision, validation, visualization, writing - review & editing.

6.Supporting Information

We have incorporated all supporting information to an associated open-access article in Data in Brief [26], which include:

1. Structures of lipids and fibrils (Figs. S1–2)
2. Structural conformations of lipids in phase-separated lipid domains (Figs. S3–5)
3. Fibril-raft binding kinetics (Figs. S6–7, Tables S1a–c, Movies)
4. Fibril membrane-bound states and orientational order in lipid rafts (Figs. S8–16)
5. Fibril-lipid minimum distance analysis (Figs. S17–28)
6. Fibril-lipid binding energy analysis (Figs. S17–22)
7. Characterizations of annular lipid shells in lipid rafts (Figs. S32–40).

Author Manuscript Author Manuscript Author Manuscript Author Manuscript

domains or GM1, with diversified membrane-bound conformations, in structurally heterogeneous lipid membranes.

Keywords

Coarse-Grained Model; MD simulations; Phase-Separated Lipid Domains; Amyloid Fibrils Membrane Interactions; Lipid Rafts; Oxidized Cholesterols

1. Introduction

Amyloid fibrils are self-assembling beta-sheet-rich peptides [1]. The membrane binding events of these fibrils to complex cell membrane surfaces have been linked to the pathogenesis of several protein aggregation disorders and diseases, e.g., neurodegenerative diseases such as Alzheimer's [2–6]. At present, the locations where fibrils bind to the cell membrane and the structure of these membrane-bound conformations are unclear. Additionally, the protein/lipid binding kinetics and energetics of these amyloid fibrils to the compositionally and structurally heterogeneous cell membranes are unknown [7, 8]. Studying fibril/lipid binding events at the molecular level may reveal the important regulatory roles of protein/lipid interactions, that trigger the subsequent fibril-induced disruption of cell membrane structure and function [9–11]. In the case of Alzheimer's, early beta-amyloid fibril interactions with the neuronal membrane, starting from the solution phase to the membrane-bound state, may contribute to progressive neuronal degeneration at the asymptomatic, or early stage of the disease [6, 8].

Beta-amyloid is highly diversified in its structure and conformation in both solution and on the lipid membrane [1, 2]. Initially, the structure of beta-amyloid is mostly in the alpha-helix form, upon its release from the cell membrane. This monomeric protein subsequently misfolds and self-aggregates to a beta-sheet-rich form, commonly known as beta-amyloid fibrils [1]. At present, the structures of beta-amyloid fibrils either in solution or in membrane-bound form on the human brain are unclear. Additionally, the key molecular mechanics underlying protein/lipid interactions of beta-amyloid fibrils on compositionally and structurally diversified neuronal membranes are unknown [2, 3, 12, 13]. Therefore, a well-defined, biologically relevant model of an amyloid fibril/membrane system is needed to explore the molecular mechanisms of beta-amyloid fibrils interactions on biologically relevant lipid membrane surfaces.

In order to study the molecular membrane-binding mechanisms of beta-amyloid fibrils with structurally and dynamically complex cell membranes, we created a fibril/membrane model system, containing beta-amyloid fibrils $(A\beta_{17–42})_n$ of increasing chain numbers, from $n = 2$ to 5, and multiple phase-separated lipid membranes with well-defined lipid domain sizes. We used an experimentally derived beta-amyloid pentamer fibrils (PDB: 2BEG) to construct our model fibrils [1]. For the membranes, we constructed several laterally, along the surface of the lipid bilayer, phase-separated membrane systems, or lipid rafts, containing saturated and unsaturated phospholipids, and cholesterol (CHOL), headgroup modified cholesterol (P4-CHOL), or tail-group modified cholesterol (C1-CHOL or P1-CHOL). In addition, a model raft with asymmetrically distributed ganglioside (GM1), a known raft marker with

Author Manuscript Author Manuscript Author Manuscript Author Manuscript

asymmetric distribution in cellular membranes, was created [14]. All lipid rafts contain liquid-ordered (Lo), liquid-disordered (Ld) and interfacial Lo and Ld, or Lod, domains, mimicking the highly structurally diversified plasma membrane of a cell [15, 16].

In order to modify the lipid domain sizes, modified sterols were created from cholesterol (CHOL) to mimic the oxysterols, i.e., cholestenone with a less polar headgroup (C1-CHOL), 25-hydroxycholesterol with an oxidized tail-group (P1-CHOL for), and 4β-hydroxycholesterol with an extra polar group (P4-CHOL for) [17]. These oxysterols play key roles in many highly regulated cholesterol oxidation pathways for cells under normal physiological or oxidative stress conditions [18–22].

To capture fibril binding behaviors from solution to membrane phase, microsecond-long coarse-grained (CG) Molecular Dynamics (MD) simulations, with multiple replicates, were employed in this study [14, 23]. CG MD simulations allow us to study molecular events in large fibril/raft complexes, ~ 20nm × 20nm × 15nm, at experimentally relevant microsecond time scales. Using CG MD, we are able to sample large regions of translational and rotational phase space more efficiently than with atomistic simulations. Here, detailed membrane binding events starting from the fibril in solution to different states including: diffusing in solution, binding to membrane surface, undergoing lateral motion, sampling different lipid phases, and exhibiting equilibrated membrane-bound states, were investigated up to 20 μs for each fibril/raft system. Overall, with *four* fibrils of different chain numbers, *three* initial positions of each fibril above the raft surface, *five* rafts of varying domain sizes, and a control (no fibril) for each raft, a total of *65* fibril/raft simulation systems were simulated, representing an accumulated ~1.3 milliseconds of simulation time in this study. Our results allow us to systematically examine the roles of fibril sizes and lipid domain structures, modulated by oxidized cholesterol and GM1, on the fibril-lipid interaction kinetics and conformation of beta-amyloid.

We have investigated the membrane binding kinetics, locations, conformation and energetics of fibril/raft complexes. The well-defined phase-separated lipid domains in our model rafts allow us to examine the domain binding preferences of fibrils upon their binding to the membrane from solution. Membrane-bound orientational states that may involve the interactions of the fibril via different binding motifs, i.e., the hydrophobic (C-terminal) and the hydrophilic (N terminal, Loop and termini) regions, to the model rafts, as well as the protein/lipid binding energy, have been carefully examined in lipid rafts with and without monosialotetrahexosylganglioside (GM1) [24]. In addition, we studied the localized effects of protein-induced structural perturbation to lipid membranes, by analyzing the lipid composition and orientational order in the annular lipid shells surrounding the membrane-bound fibrils.

The results of this microsecond-MD simulation study reveal molecular details of the binding locations, kinetics, membrane-bound conformations, and energetics of amyloid-fibrils to structurally diversified lipid membranes. This study may provide insight on the roles of lipid domains in regulating the initial fibril binding events to cell membranes. In addition, the observed membrane-bound conformation of beta-amyloid fibril from our equilibrated MD

Author Manuscript Author Manuscript Author Manuscript Author Manuscript

simulations, may be useful for developing markers and drugs that can detect and inhibit the cytotoxicity of amyloidogenic protein at the early pathogenesis of Alzheimer's [25].

2. Methods

2.1. Coarse-grained lipid rafts

The construction and design of our initial ternary lipid raft systems were based on a previously published, fully hydrated and equilibrated 3-component CG-lipid raft model [23]. This raft system contains 828 saturated dipalmitoylphospatidylcholine (DPPC), 540 polyunsaturated dilinoleoylphosphatidylcholine (DLPC), 576 cholesterol (CHOL), and 12600 waters, with the lipid molar ratio of DPPC:DLPC:CHOL = 0.42:0.28:0.30.

As reported by Risselada and Marrrink [23], their ternary lipid raft system was constructed from randomly distributed lipids at time zero. After 2.5μs of CG simulation time, or an effective time of 10 μs based on the ~ 4 times faster diffusion time of CG-water than that of atomistic water, the lipid rafts established phase-separation [23]. The CG and atomic chemical structures of each lipid are demonstrated in Fig. 1 and Fig. S1 [26], respectively. Note that this ternary lipid bilayer system exhibits lateral (along the bilayer surface) phase separation with DPPC-rich Lo, DLPC-rich Ld and interfacial Lo/Ld or Lod domains [23], and it serves as our control raft system, CO-raft. In addition, this system serves as our lipid membrane design template for the other four lipid raft systems containing modified cholesterol and asymmetrically distributed GM1 lipids as described below.

We have constructed three ternary lipid rafts by modifying the polarity of the CHOL headgroup (ROH) or tail-group (C1) CG-atom of the cholesterols in the control CO-raft creating: C1-raft (DPPC:DLPC:C1-CHOL), P1-raft (DPPC:DLPC:P1-CHOL) and P4-raft (DPPC:DLPC:P4-CHOL), all with identical molar ratios as the CO-raft. Fig. 1 demonstrates the atom types of C1-CHOL, P1-CHOL and P4-CHOL when compared with CHOL. The chemical structures of oxidized cholesterols, or oxysterols, corresponding to these modified CG-cholesterols are illustrated in Fig. S1 [26].

To create the C1-raft, the polar SP1 atom type of the headgroup ROH of CHOL in CO-raft (Fig. 1D) was changed to a less polar atom type C1 to create C1-CHOL (Fig. 1E), and to create the P4-raft, SP1 was changed to a more polar atom type P4 to create P4-CHOL (Fig. 1G). Finally, to create the P1-raft, the non-polar C1 atom type of the tail-group C1-CHOL in CO-raft (Fig. 1D) was changed to a polar atom type P1 to create P1-CHOL (Figs. 1F). The polarity of the CG atom type increases from C1, SP1, P1 to P4, based on the computed free energies of hydration of model CG-compounds, as described in the Martini CG model [27, 28].

A quaternary GM-raft with asymmetrically distribution GM1 lipids was created by replacing some lipids of only one lipid monolayer with GM1-lipids (Fig. 1C) in the CO-raft, while keeping the surface area of each lipid monolayer in the equilibrated CO-raft the same. To create the GM-raft, 119 DPPC, 53 DLPC and 166 CHOL in one lipid monolayer of the CO-raft were removed and replaced by 36 GM1 lipids, resulting in the final lipid molar ratio of GM1:DPPC:DLPC:CHOL = 0.02:0.43:0.30:0.25.

Author Manuscript Author Manuscript Author Manuscript Author Manuscript

The above five lipid raft systems, CO-raft, C1-raft, P1-raft, P4-raft and GM-raft, represent our model raft systems in this study.

2.2. Coarse-grained fibrils

Atomistic beta-amyloid fibrils $(A\beta_{17–42})_n$ of four different chain lengths (n = 2 to 5) were constructed from the experimentally derived NMR structure (PDB ID code 2BEG) [1] of human beta-amyloid, or ABCDE with 5 peptide chains. The coordinates of the disordered residues 1–16 are missing in the experimental NMR structure. The available coordinates for residues 17–42 for each chain, with primary sequence: LVFFA**ED**VG**SNK**GAIIGLMVGGVVIA, are given in the PDB data, with the polar residues are highlighted in bold. This pentamer exhibits a highly ordered β-turn-β motif of each fibril chain (Fig. 2 and Fig. S2 [26]). By deleting one, two or three chains from the 5-chain pentamer fibril, tetramer (ABCD with 4 chains), trimer (ABC with 3 chains) or dimer (AB with 2 chains) fibril, respectively, were constructed. Fig. 2 shows the assigned chain labels (based on the primary sequence above) and residue locations, or #'s, starting from #1–26 for chain A, #27–52 for chain B, #53–78 for chain C, #79–104 for chain D and #105–130 for chain E, of the smallest (dimer AB) and the largest (pentamer ABCDE) fibrils.

As shown in Fig. 2A, chain A of the fibrils contains an N-terminal (#1–10), a loop (#11–15) and a C-terminal (#16–26). Interestingly, only the N-terminal and half of the loop regions contain polar or charged residues, #6 (E22), #7 (D23), #10 (S26), #11 (N27) and #12 (K28), while half of the loop region and the entire C-terminal contain hydrophobic residues. The same structural and hydrophobicity profile apply to the other fibril chains. Other than the inter-chain hydrogen-bonding along the parallel beta-sheets, an inter-chain salt bridge between K28 and D23 also helps stabilize the fibril structure (Fig. S2 [26]). These atomistic fibril structures were used to create the CG-fibrils in this work. CG-fibrils were constructed from atomistic fibril structures using the atomistic-to-CG program, martinize.py [29], based on the MARTINI protein force field [30] combining an elastic network force field [31] for stabilizing the fibril chains. Fig. 2 shows the CG-fibril structures overlaid on the atomistic structures of the dimer and tetramer fibrils. It is clear that the CG-beads successfully represent the atoms of both the backbone and sidechains for all fibril sizes.

2.3. Simulations of rafts and fibrils

Creation of the simulation box and addition of water and ions were performed. Each raft or fibril system was separately immersed in a box of water and monovalent ions using GROMACS tools [32], *pdb2gmx*, *editconf*, *genbox*, and *genion*. The number of ions in each system was just enough to neutralize the system. The hydrated system then underwent 500 steps of energy minimization using steepest descent to get rid of the potential water and ion overlaps with the lipid or protein atoms.

After energy minimization, a short 2 ns pre-equilibration, i.e., position-restrained MD simulation, was then performed. This step is important to improve simulation stability and eliminate local high energy structures creating during the solvation and ion addition steps. Here, the lipid or fibril CG atoms were position-restrained using harmonic potentials with spring constants of 1000 kJ mol^{-1} nm^{-2} along the x, y and z directions. Periodic boundary

Author Manuscript Author Manuscript Author Manuscript Author Manuscript

conditions were applied on each x, y and z directions. Bond lengths were constrained by a linear constraint solver (LINC) algorithm [33]. Long range electrostatic interactions were estimated by Particle Mesh Ewald method [34]. Nonbonded interactions were cut off at 1.2 nm, and potential shifts at 0.9 and 0.0 nm for the Leonard Jones and Coulomb interactions, respectively. Semi-isotropic pressure coupling was achieved using the Berendsen barostat[35] with a coupling constant of 2 ps for maintaining the pressure of 1 bar. Temperature coupling was performed using the v-rescale thermostat [36] with a coupling time of 1 ps to maintain a temperature of 310K. Note that constant temperature baths were coupled to lipid, protein and combined water and ion groups separately for improving the thermal coupling accuracy and efficiency for our large simulation complex. A leapfrog integrator algorithm[37] with a 20 fs time step was employed to integrate the motion of the atoms. All MD simulations in the NPT ensemble were performed using MARTINI CG force fields Version 2.20 for proteins and lipids[27, 29] and ran on GROMACS [32].

Finally, the pre-equilibrated lipid raft and fibril systems underwent non-restrained, or production, MD simulations separately for 3 and 1 μs, respectively, using the MD parameters described above, without position restraints. The equilibrated structures of rafts and fibrils represent the initial structures for constructing the fibril/raft complexes.

2.4. Simulations of fibril/raft complexes

Simulations of fibril/raft complexes with replicates involves three steps: alignment of the fibril above the lipid raft, creation of simulation replicates by translating the fibril laterally along the bilayer, and production MD simulations of the replicates.

For the alignment of fibrils, each hydrated and equilibrated fibril was aligned based on the calculated molecular principal axes of gyration (X, Y and Z) using the tool, *g_gyrate* from GROMAS [32]. Here, the fibril Y axis corresponds to the axis of gyration with the smallest radius of gyration of the molecule, or along the symmetric long axis of the fibril chains, i.e., from the N-terminus to the loop and the loop to the C-terminus. The fibril X and Z axes correspond to the axes of gyration with larger radii of gyration and orthogonal to the fibril Y-axis. The design rationale of the fibril alignment was to match the molecular axes (X, Y, Z) of each fibril with the simulation axes (x, y, z) of the lipid raft, in which both the Z-axis of the fibril and the z-axis of the simulation box is perpendicular to the plane of the lipid bilayer as shown in Fig. 3F.

Three different simulation replicates (1 to 3), corresponding to three different positions of the aligned fibril along the z-y plane of the raft were created in the solution phase. Here, the center of the replicate 1 was at (0, −5nm, 5 nm), replicate 2 at (0, 0, 5nm) and replicate 3 at (0, 5nm, 5nm), with respect to the center (0, 0, 0) of the lipid raft, as demonstrated in Fig. 3F.

After the sequential steps of alignment of fibril and creation of simulation replicates of each fibril/rat complex, each assembled complex underwent energy minimization similar to the steps as shown above but in the presence of additional monovalent ions to create an overall 0.1 M of NaCl, a biologically relevant environment in a protein/membrane system. Afterwards, a 2ns pre-equilibration as described above was performed. Overall, the size of

Author Manuscript Author Manuscript Author Manuscript Author Manuscript

the final fibril/raft system is ~ 22 × 22 × 13 nm^3 for the ternary rafts, but ~ 21 × 21 × 14 nm^3 for the quaternary raft. About 36,000 CG water molecules are present in each raft. Finally, each replicate of the fibril/raft system underwent 20 μs of simulations in the NPT ensemble as described above. Note that additional controls, i.e., rafts but in the absence of fibrils, were also prepared and simulated under identical pre-equilibration and simulation conditions as the fibril/raft complexes.

2.5. Characterizations of lipid domains

A data-filtering tool, *g_select*, from GROMACS [32] was used to classify lipids into three lipid domains: Lo, Ld, and Lod. The Lo domain, representing the DPPC-rich domain, consists of DPPC lipids for which all atoms are beyond 0.5 nm of any atom of another DPPC lipid. The Ld domain, representing the DLPC-rich domain, consists of DLPC lipids for which all atoms of these lipids are beyond 0.5 nm of any atom of another DLPC lipid. The Lod domain consists of DPPC molecules that are not included in Lo domain and DLPC molecules that are not included in Ld domain. Finally, Lo-CHO, Ld-CHOL, and Lod-CHOL represent groups of CHOL, for which all atoms are within 0.5 nm with the lipids in Lo, Ld and Lod domains, respectively. Fig. 3 demonstrates the domain structure of several rafts.

The average transverse (along the lipid bilayer normal, or z-axis) density profile, or number density $\rho_N(z)$ vs. z, of various structural groups of lipids, such as the polar headgroup or hydrophobic lipid chain tailgroup, within each Lo, Ld and Lod lipid domain, was calculated using the tool, *g_density*, from GROMACS [32]. Here,

$$\rho_N(z) = \frac{1}{N}\sum_{i=1}^{N}\frac{n_i(z)}{A\Delta z}, \tag{1}$$

where $n_i(z)$ is the number of a selected lipid group within a thin z-slice of thickness ΔZ at a given z-coordinate at the i^{th} time frame, A is the cross-sectional (x-y) area of the raft, N is the total number of time frames used for the calculation. In this study, $\Delta Z = Z_s/100$, where Z_s is the Z-dimension of the simulation box.

The time-averaged lipid order parameter $S(n)$ for a given chain carbon number position (n) was calculated using the tool, *g_order*, from GROMACS [32]. $S(n)$ measures the segmental orientational order of the lipid or protein chain with respect to the z-axis, normal of the bilayer,

$$S(n) = \frac{1}{N}\sum_{i=1}^{N}\left\langle\frac{3cos^2\theta_n - 1}{2}\right\rangle, \tag{2}$$

where θ_n represents the angle between the z-axis and a vector C_n (= r_{n+1} - r_{n-1}) joining the two nearest-neighboring on each side of the n^{th} chain carbon atom, where r_{n+1} and r_{n-1} are the position vectors of the n+1 and n-1 chain carbon positions of each lipid chain [38]. Also, N is the number of time frames for the time-averaging.

In our CG DPPC, DLPC and GM1, each lipid acyl chain has 4 CG atoms, e.g., C1A to C4A of the sn-1 chain of DPPC (Fig. 1A). Therefore, two order parameters were determined for

Author Manuscript Author Manuscript Author Manuscript Author Manuscript

each chain. For simplicity, the average of the four order parameters, two from each chain, was used to define the order parameter of each lipid. For the cholesterol and modified cholesterol, a single θ represents the angle between the long axis of cholesterol, defined by the vector starting from the last CG atom (R5) to the first CG atom (R1), and z-axis, was used to determine the cholesterol or modified cholesterol order parameter, or the tile of the cholesterol long axis, with respect to the normal of the lipid bilayer. as shown in Figs. 1D–G.

In our CG-fibrils, the peptide backbone atoms were used to calculate the order parameter $S(n)$, where n is residue number of the fibril. Instead of plotting the 2D time-averaged $S(n)$ vs. n, a 3D $S(n)$ vs. time was generated to examine the time evolution of fibril orientation profile.

The surface area and area per lipid in each lipid phase were also estimated using the published GridMAT-MD program [39], which was based on a 2D-grid projection method. First, we calculated the lateral surface area occupied by each DPPC or DLPC lipid in the lipid bilayer, according to the coordinates of the phosphate atom location of each lipid. Based on the classification of Lo, Ld or Lod of each lipid from our calculation using the g-select tool of GROMACS [32], the lateral surface areas of the DPPC-rich Lo, DPPC-rich Ld and Lod domains were subsequently estimated.

Since the lateral locations of CHOL headgroups strongly overlap, or are close to the headgroups of DLPC and DPPC, the area per lipid for CHOL cannot be determined separately by GridMAT-MD. However, CHOL is effectively covered by PC headgroup and has the known condensing effect in lipid bilayer. [40] The area per lipid in each phase is then determined by the lateral surface area obtained above divided by the total number of lipids in each phase. Our calculations are: Area per lipid in Lo = lateral surface area of Lo/(total number of Lo-DPPC and LoCHOL), Area per lipid in Ld = lateral surface area of Ld/(total number of Ld-DPPC and LdCHOL), and Area per lipid in Lod = lateral surface area/(total number of Ld-DPPC, Lo-DLPC and Lod-CHOL).

2.6. Characterizations of annular lipids

The same *g_select* tool [32] was used to characterize annular lipid shells from each fibril/raft system. In this case, if an atom of any lipid (DPPC, DLPC, CHOL or modified CHOL, or GM1) is within 0.5, 0.5–1.0, 1.0–2.0 and 2.0–3.0 nm from an atom of a fibril, that lipid is then assigned to annular lipid shell 1, 2, 3 and 4, respectively. Once the annular lipid shells are identified, the transverse profile and order parameter of lipids in each shell can be calculated using the same methods as above.

2.7. Analysis of fibril-lipid binding energetics, conformation, kinetics and location

The time averaged non-bonded interaction energy between the fibril and each lipid group over a period of time was calculated using the tool, *g_energy*, from GROMACS [32] for each fibril/raft complex.

The time-evolution and final membrane-bound conformation of each fibril and the surrounding lipid shell throughout the entire 20 μs simulation for each replicate was determined using Visual Molecular Dynamics program (VMD) [41].

Author Manuscript Author Manuscript Author Manuscript Author Manuscript

Quantitative information of the fibril binding kinetics and location of the fibril/lipid interaction was obtained from the minimum-distance statistical analysis using the tool, *g_mind*, from GROMACS [32]. Three different statistical analysis: (1) the time-dependent fibril-lipid minimum distance, defined as the minimum distance between any atom of the fibril and any atom of a lipid group, vs. time, (2) number of atom contacts within a certain distance threshold vs. time, and (3) the minimum distance vs. protein residue location averaged over a period of time, or "residue-contact plot", were obtained for each fibril/raft complex. The minimum distance and number of contacts vs time plots allow us to accurately determine the kinetics of fibril binding in terms of the time event and particularly the time of contact, or binding time, of the fibril with respect to each lipid, DPPC, DLPC, CHOL or modified CHOL, or GM1. On the other hand, the "residue-contact plot" provides important information of the nearest-neighbor lipids surrounding the fibril upon forming a stable membrane-bound state. Note that this residue-contact map and the VMD analysis provides the basis for determining the binding location of the fibril in each fibril/raft complex and establishes the domain preference, ie., Lo, Ld or Lod, of the fibril in the model raft.

Other than the conventional 2D fibril-lipid minimum distance vs. time plot and direct visualization of binding events based on VMD, plots of 3D fibril-lipid minimum distance vs. residue and vs. time was also generated. This 3D fibril-lipid minimum plots, together with the 3D protein $S(n)$ vs. n and vs. time, were also used to quantify the binding events of fibril in all lipid rafts. This multiple parameter characterization approach of fibril binding provides useful information about the binding kinetics from solution to membrane-bound state, assignment of equilibrated membrane-bound state, and the stability of each membrane-bound state in this study

3. Results

3.1. Characterizations of Lo, Ld and Lod lipid domains

In the absence of fibrils, phase-separated DPPC-rich Lo domain, DLPC-rich Ld domain, and mixed DPPC and DLPC at the interfacial Lo/Ld, or Lod domain, were characterized in the CO-raft, C1-raft, P1-raft, P4-raft and GM-raft. As described in Methods, Lod domain is made up of DPPC not belonging to Lo domain and DLPC not belonging to Ld domain. It is clear from the lateral (x-y) views (Fig. 3A–E) that distinct phase-separated lipid domains were detected in the CO-raft, P1-raft, P4-raft and GM-raft, but poorly resolved domains were found in the C1-raft. For the case of GM-raft, surface clusters of GM1 on one lipid monolayer were clearly associated with the Lo-domain (Fig. 3E). CHOL in the CO-raft and the GM-raft, as well as the modified CHOL (P1-CHOL in the P1-raft and P4-CHOL in the P4-raft), partition mostly in the Lo-domain than in the Ld domain. However, the less polar headgroup modified CHOL (C1-CHOL) distributed evenly within the entire lipid bilayer (Fig. 3B).

Binding of beta-amyloid fibrils from solution at time zero to the lipid bilayer surface was observed in all *60* simulation replicates. These replicates include *four* fibrils with different chain numbers (from dimer to pentamer), on *five* lipid rafts, and *three* different initial positions of fibrils (Fig. 3F). Due to the periodic z-boundary condition, each fibril sees the upper and lower monolayers of the lipid bilayer, as demonstrated in Figs. S6–7 [26]. Note

Author Manuscript Author Manuscript Author Manuscript Author Manuscript

the fibril is closer to the upper monolayer (~ 2.5 nm from the surface), than the lower monolayer by design. Interestingly, attachment of the fibril to either the upper or lower monolayer was evident at different binding times as summarized in Tables S1a–c [26]. The results indicate sufficient sampling of the rotational and translational phase space in solution and on bound state for all fibrils throughout the long 20 μs simulation time in this work. In addition, movies generated from VMD [41] demonstrating the fibril/raft interaction events from fibril in solution at time zero including: undergoing fast motion in the solution phase before anchoring to membrane surface, initial binding to membrane surface, undergoing slower lateral diffusion on membrane surface, and finally exhibiting stable membrane-bound state, are given in supporting document [26].

Upon the fibrils binding to the rafts, similar lipid domain structures and CHOL partitioning behavior were observed for all fibrils when compared with the control, i.e., the same lipid raft without fibrils but simulated under identical pre-production and production run. Here, binding of the dimer binding is shown (Figure 4A–E, columns AB). Fig. 4 also highlights the Lod domain (dark green and dark orange) that define the boundary of Lo (light green) and Ld (light orange) domains for the non-GM-containing and GM-rafts (Figure 4 K–P). Once again, the light green and light orange regions are clearly resolved in all rafts, except the C1-raft, agreeing with the results before the fibril binding (Fig. 3L). In addition, Fig. 4 further demonstrates that the dimer fibril binds exclusively to the Lod domain in all non-GM containing lipid rafts.

To obtain quantitative information about the relative sizes of the phase-separated domains of the lipid rafts, the lipid compositions of each resolved Lo, Ld, or Lod domain in each fibril/raft complex were determined. Here, the percentages of DPPC, DLPC, CHOL and modified CHOL in each lipid domain were determined using the *g_select* tool [32] (see Methods). Fig. 4 shows the accumulated percentage histograms for all five rafts in the absence (control) and presence of fibrils of all sizes from dimer to pentamer, i.e., AB, ABC, ABCD and ABCDE, and all simulation replicates (1–3). The results show the average over the last 5 μs of the 20 μs simulation for each lipid raft. Significantly different lipid composition profiles were observed among different fibril/raft complexes. However, for each fibril/raft complex, the presence of bound fibril did not perturb the lipid composition profile of each lipid domain for all fibril sizes and for all simulation replicates when compared with the control. The uncertainty or SE of mean from the percentage calculation is ~ 2%.

For the cholesterol (CHOL or modified CHOL), the CHOL% in the Lo-domain of each rafts decreases from P4-raft, CO-raft, GM-raft, P1-raft to C1-raft, with ~ 74%, 65%, 60%, 49% to 39%, respectively (Figs. 4). On the other hand, the values of CHOL% in the Ld domain are relatively small and constant (within the 2% uncertainty), i.e., ~ 9%, 12%, 10%, 11% and 7% for P4-raft, CO-raft, GM-raft, P1-raft and C1-raft, respectively. Interestingly, the ranking order of CHOL% in the Lod domain of each raft is identical to that of CHOL% in the Lo domain with ~ 18%, 23%, 30%, 40% to 55%, accordingly.

For the phospholipids, the ranking of DPPC% in the Lo-domain, or Lo-DPPC%, decreases from P4-raft, CO-raft, GM-raft, P1-raft to C1-raft, with ~ 33%, 29%, 22%, 18% to 10%, respectively (Fig. 4). On the other hand, the DLPC% in the Ld-domain, or Ld-DLPC%, is

Author Manuscript Author Manuscript Author Manuscript Author Manuscript

always lower than the Lo-DPPC% for each raft and decreases ~13%, 10%, 8%, 5% to 2% following the same ranking order as above. Finally, Lod-PC%, representing the sum of DPPC% in Lod and DLPC% in Lod, is larger than Lo-DPPC% or Ld-DLPC% in all rafts. Here, Lod-PC% increases from 54%, 61%, 70%, 77% to 88%, again following the same ranking order as above.

Other than percentage distribution of each lipid species in three separated lipid domains, the relative lateral surface area of each lipid domain, as well as the area per lipid and cholesterol % (= cholesterol/total lipid x 100), were determined (Figure S3 [26]). The ranking of the surface area and area per lipid is similar to the lipid percentage ranking as shown above. In addition, the cholesterol % follows the order of Lo > Ld and Lod for CO-raft, P4-raft and GM-raft. However, the cholesterol % in Lo and Ld are similar in C1-raft and P1-raft.

The transverse views (x-z) of the rafts are shown to emphasize the distributions of the headgroups and tail-groups of the CHOL or modified CHOL within the hydrophobic region of the lipid bilayer (Fig. 5). Here, the ROH headgroup (red sphere) is polar for CHOL, P1-CHOL and P4-CHOL, but non-polar for C1-CHOL. Also, the C2 tail-group (blue sphere) is non-polar for CHOL, P4-CHOL and C1-CHOL, but polar for P1-CHOL. With the modified polarity, the headgroup ROH of CHOL (red) is mostly found near the polar region of the lipid bilayer, as represented by the polar groups of DPPC (green) and DLPC (orange), in the CO-raft (Fig. 5A). Similar observation was found in the P4-raft or GM-raft (Figs. S4 [26]). Also, the fused ring region (Figs. 1 and S1 [26]), in the form of ellipsoid (black), of CHOL or P4-CHOL, is aligned mostly parallel to the bilayer normal for the CO-, P4- and GM-rafts. However, the non-polar ROH headgroup of C1-CHOL clearly avoids the polar region of the lipid bilayer and distributes itself around the center of the bilayer in the C1-raft (Fig. 5B). Interestingly, the dual-polar, i.e., polar ROH headgroup and polar C1 tail-group, is found in both the center and near the PC headgroup in the P1-raft (Fig. 5C).

The cholesterol distribution behavior within the hydrophobic region of the lipid bilayer can further be quantified using the transverse number density profile as shown in Figs. 6 and S4 [26] Here the number density vs. z distance along the normal of the lipid bilayer surface plots for the headgroup ROH and tail-group C2 of CHOL or modified CHOL were demonstrated. Same as above, the polar region of the lipid raft is represented by the polar PO4 of DPPC in the Lo domain (upper panel), PO4 of DLPC in the Ld domain (middle panel) and PO4 groups of PC in the Lod domain. Clearly, the peaks of polar ROH headgroup of CHOL and P4-CHOL are distributed near the PO4 peaks of PC in all domains, while the non-polar C2 tail-group of CHOL are found at the center of the bilayer in the CO-raft (Fig. 6A). Similar observation was found for P4-raft (Fig. S4C [26]) and GM-raft (Fig. S4D [26]). In contrast, both ROH and C2 of C1-CHOL are found in the middle of the lipid bilayer of the C1-raft (Fig. 6B). Interestingly, a broader, trimodal distribution, consisting of two poorly resolved peaks near the PO4 peaks of PC for either ROH and C2 of P1-CHOL and a peak at the center of the bilayer, are found in the P1-raft (Fig. 6C).

The order parameters of lipids, DPPC, DLPC and cholesterol (CHOL or modified CHOL), measure the alignment or orientational order of the lipid acyl chain segments of DPPC or DLPC and the long axis of cholesterol (Fig. 1) with respect to the normal of the lipid bilayer.

Author Manuscript Author Manuscript Author Manuscript Author Manuscript

Here, the average order parameters of lipids over the last 5 μs in each lipid domains have been determined.

For the cholesterol (Figs. S5A–C [26]), the order parameter of the long axis in the Lo domain is highest, becomes lower in Lod domain, and even lower in the Ld domain. In addition, the order parameter of C1-CHOL in the C1-raft is very low, ~ 0.1 in Lo, - 0.05 in Ld and 0.05 in Lod, when compared with those of CHOL, P1-CHOL or P4-CHOL in other rafts. In general, the order parameter in all three domains, follows the ranking order of P4-raft, CO-raft, GM-raft, P1-raft to C1-raft. These results support the observed distinctly different headgroup and tail-group transverse distribution behaviors of CHOL or modified CHOL in different rafts noted above. Specifically, the long axis of P4-CHOL preferentially aligned along the bilayer normal, but C1-CHOL preferentially aligned parallel to the bilayer surface. The presence of fibrils did not alter the order parameter significantly in each phase-separated domain.

For the DPPC (Figs. S5D and E [26]) and DLPC (Figs. S5F and G [26]), the acyl chain order parameter of DPPC is higher in the DPPC-rich Lo domain than in mixed DPPC and DLPC Lod domain. Conversely, the order parameter of DLPC is slightly higher in the Lod than in the Ld domain. The order parameter of either DPPC or DLPC is lowest in C1-raft when compared with the same parameter in other rafts. Same as cholesterol, the presence of fibrils did not perturb the order parameter of either DPPC or DLPC in each phase-separated domain.

3.2. Membrane-bound conformation and binding kinetics of fibrils in lipid rafts

The membrane-bound conformation and binding kinetics of fibrils of various sizes in the CO-raft, C1-raft, P1-raft, P4-raft and GM-raft were examined. Results of the first four rafts, i.e., non-GM-rafts, will be presented first, followed by the results of the unique, asymmetric GM-raft.

Membrane-bound conformation, or state, of each fibril in the lipid raft has been examined using VMD. As described in Methods and Fig. 1, each fibril has three distinct regions: N-terminal, C-terminal and Loop. At the end of the 20 μs simulations, the region of the fibril that came in closest contact with the membrane surface is used to classify the membrane-bound state. Fig. 7 shows the representative membrane-bound states from four simulation replicates. CO-ABCD-2 (C-state), CO-ABCD-3 (T-state), C1-ABC-3 (N-state), and P1-ABC-2 (I-state). For the C-state of the CO-ABCD-2 replicate (Fig. 7A), the longer and hydrophobic C-terminal of the fibril was clearly embedded into the lipid monolayer. For the T-state of the CO-ABCD-3 replicate (Fig. 7B), both N-terminus and C-terminus came into contact with the membrane surface while the long axis of the fibril was tilted towards the normal of the bilayer. For the N-state of the C1-ABC-3 replicate (Fig. 7C), the shorter and hydrophilic N-terminal was embedded into the lipid monolayer. Lastly, for the I-state of then P1-ABC-2 replicate (Fig. 7D), both C-terminal and N-terminal were inserted into both leaflets of the bilayer and exhibited a transmembrane configuration.

Other than VMD visualization, both 3D protein order $S(n)$ vs n vs time plot (Fig. S13 [26]) and time-averaged $S(n)$ vs n over the last 5 μs (Fig. S15 [26]) were generated to evaluate the

Author Manuscript Author Manuscript Author Manuscript Author Manuscript

time-evolution and stability of the membrane-bound states. For the case of C- or N- state, low order parameter of the C- and N-terminal residues but high order parameter of the loop region is evident. On the other hand, for the case of T-state, the above trend is just reverse, as the C- and N-terminal are of high order, aligned towards the z-axis, while the loop region aligns more along the membrane surface or perpendicular to the z-axis.

Table 1 summarizes the assignments of membrane-bound states of all replicates in the lipid rafts. Interestingly, the dimer fibril remains exclusively in the C-state in all the lipid rafts. However, for larger fibrils, multiple T states and N states were observed in the C1-raft and P4 raft. A single T-state in the CO-raft, and one I-state and one N-state in the P1-raft were found.

Figs. S8–11 [26] show the membrane-bound conformation and the assigned state of all 48 replicates of the non-GM1 containing lipid rafts.

In addition to generating qualitative descriptions of membrane-bound conformations using VMD, a quantitative minimum-distance statistically analysis (see Methods) was employed. Here, three different plots have been generated for the same four fibril/raft complexes as described above (Fig. 8). First, the binding kinetics of fibrils in terms of the minimum distance between the fibril atoms and the lipid atoms vs. simulation time (upper panel) provides the binding kinetic information of the association of the fibril with individual lipid species, DPPC, DLPC or CHOL. Second, the number of fibril atoms and lipid atoms, satisfying the proximity criterion of less than 2 nm, vs. simulation time (mid panel) describes the extent of fibril interaction with the lipid membrane. Finally, the average minimum distance between the fibril atoms and lipid atoms over the last 5 μs vs the residue number of fibril (lower panel) represents a measure for assigning membrane-bound state for each simulation replicate.

For the representative C-state in CO-ABCD-2 (Fig. 8A), both the abrupt drop in the minimum distance (upper panel) and the concomitant increase in the number of contacts (mid panel) vs. time plots indicate that the fibril established contact and bound to lipid membranes at around 4.2 μs. Also, the regions with a minimum distance around 0.5 nm overlapped with the C-terminal regions of all three fibril chains in the minimum distance vs. fibril residue plot (lower panel) agree with the direct observation of the C-state as given in Fig. 7A.

For the T-state in CO-ABCD-3 (Fig. 8B), establishment of stable fibril binding occurred at around 0.45 μs (upper and mid panels), whereas the minimum distance vs. fibril residue (lower panel) shows regions of contact overlapping the C- and N-termini of the fibril. For the N-state in C1-ABC-3 (Fig. 8C), stable binding occurred at about 0.7 μs (upper and lower panels) and the fibril/lipid contact regions overlapped with the N-terminal (lower panel). Finally, for the I-state in P1-ABC-2 (Fig. 8D), stable binding occurred at around 0.3 μs (upper and lower panels). Interestingly, close contacts were established for chains A and C with DPPC and DLPC, however, portions of the N-terminal and loop regions of chain B did not come on close contact with either DPPC or DLPC. Unlike DPPC and DLPC, cholesterol had contact with the all three fibril chains mainly in the N-terminal region. The quantitative

Author Manuscript Author Manuscript Author Manuscript Author Manuscript

three-panel minimum distance analysis plots of all replicates in non-GM rafts are shown in Figs. S17–20. [26] Using the abrupt drop in the minimum distance vs. time plot, the time of fibril binding time to each lipid for each non-GM-rafts was determined, and the results are shown in Table S1a–b. [26]

Other than the use of a 2D fibril-lipid minimum distance vs. time plot to quantify the binding time, a 3D fibril-lipid minimum distance vs. fibril residue vs. time for each lipid was also generated to quantify the residue-specific binding kinetics events of the fibrils (Figs. S23–24 [26]). We observe good agreement between the 2D plot and 3D plots.

Similar to the non-GM-rafts, binding conformation and kinetics of fibrils in the GM-raft have also been investigated. Here, the role of surface GM1 cluster, asymmetrically located on one lipid monolayer, or top monolayer which faced the protein the solution phase before the simulations, of GM-raft, in regulating the fibril binding behaviors was examined.

The dimer binding to the GM-raft exhibits interesting membrane-bound conformations and kinetics. Similar to the above non-GM1 containing raft, the dimer fibril bound to the raft membrane surface involving the C-terminal in all three replicates as shown in Table 1 and Fig. 9. Among them, two replicates, GM-AB-1 and GM-AB-2, associated strongly with the surface GM1 headgroups, binding via all regions of the protein including: the N-terminal, loop regions, and C-terminal. Therefore, these two replicates were labeled as an S-state, indicating surface binding of the fibril to the GM1 headgroup on the membrane surface as demonstrated in Fig. 9B. Interestingly, the dimer fibril in the third replicate, GM-AB-3, migrated to the non-GM1-containing or “bottom” monolayer, i.e., the lipid leaflet on the opposite side of the initial protein-facing leaflet, in less than 0.1 μs (see Table S1c [26]). Subsequently, this dimer bound strongly to this bottom leaflet via the C-terminal in the same fashion as the dimer binding to the non-GM1 containing raft as demonstrated in Fig. 9A. Therefore, this replicate is labeled as C-state, but does not involve extensive binding to surface GM1 headgroup like the other two replicates.

Similar to the non-GM-rafts, both 3D protein order $S(n)$ vs n vs time plot (Fig. S14 [26]) and time-averaged $S(n)$ vs n over the last 5 μs (Fig. S16 [26]) were generated to evaluate the time-evolution and stability of the membrane-bound states. These calculations confirm the stability of the membrane bound states and the assigned membrane-bound states.

For the larger fibrils, a multitude of distinct membrane-bound states were observed (Figs. 9 and S11 [26]). Here, the C- and N-states that involve direct binding to the surface GM1-cluster are shown in Fig. 9C and Fig. S12D [26], respectively. A new L-state was observed in GM-ABCD-2, where the loop region of the tetramer fibril landed on the GM1 headgroup, with the fibril long axis aligned along the normal to the bilayer as shown in Fig. 9D. Note, the fibril alignment of the L-state is opposite to the alignment of the T-state, in which the fibril bound at the terminus, on the opposite end of the loop along fibril long axis. In addition, binding of a pentamer fibril to the bottom layer without GM1 was also found in the GM-ABCDE-2 replicate as a C-state as shown in Fig. S12K [26]. The membrane-bound orientation of this C-state in the absence of binding to the surface GM1 is again similar to the C-state of GM-AB-3 and other C-states found in non-GM-rafts.

Author Manuscript Author Manuscript Author Manuscript Author Manuscript

Similar quantitative minimum distance statistics was used to determine the fibril binding kinetics and conformation analysis for the GM-raft. Fig. 10 demonstrates the minimum distance analysis for the same four replicates, GM-AB-3 (C-state), AB-2 (S-state), ABCD-1 (C-state) and ABCD-2 (L-state). Comparing the 3-panel plot of GM-AB-3 (Fig. 10A) with that of GM-ABCD-1 (Fig. 10C) clearly shows that GM1 did not participate in fibril binding in AB-3, but did so in ABCD-1, consistent with the observations as described above. Surprisingly, the dimer established intermittent contact with the acyl chain groups of GM-1 throughout the entire 20 μs simulation, as shown in the minimum distance and number of contacts vs time plots in Fig. 10A. From the minimum-distance vs time plots, we observed that fibril binding to the GM1happenned at different time points, and the fibril did not always bind directly from solution to GM1 in GM-rafts. For example, in GM-AB-2 (Fig. 10B), fibril binding to GM1 occurred very early within the first 0.3 μs, and fibril binding to other lipids was established later at ~ 2.5 μs. However, in GM-ABCD-1 (Fig. 10C), the fibril bound to the non-GM1-region on the upper monolayer, or the monolayer containing GM1, in less than 0.2 μs. Upon establishing the lipid membrane binding, GM1 binding occurred much later at ~ 2 μs. Minimum distance binding analysis of all replicates of GM-rafts are shown in Fig. S21 [26]

Additionally, 3D fibril-lipid minimum distance vs. fibril residue vs. time for each lipid were generated to quantify the residue-specific binding kinetics events of the fibrils (Figs. S25–28 [26]). We also observe good agreement between the 2D plot and 3D plot representations.

3.3. Energetics of fibril/lipid interactions in lipid rafts

The binding energies of all membrane-bound conformations were calculated to compare the energetics of the most common C-state to the rarer N-State, T-State, L-State and I-States (Fig. S17 [26]). In the non-GM1 containing rafts, the fibril-raft binding energies were ~ −200 to −800 kJ/mol for DPPC and CHOL, and ~ −100 to −600 kJ/mol for DLPC. In general, for either DPPC or cholesterol (CHOL and modified CHOL), the fibril/lipid binding energies was significantly higher in the T- or N-state than in the C-state for fibrils of the same size in each non-GM1 containing raft, except the P1-ABCD-1 replicate. Similar observation was also found in the total binding energy, i.e., sum of individual fibril/lipid binding energies. However, for the I-state of P1-ABC-2, the fibril/P1-CHOL binding energy was ~ −800 kJ/mol, representing the lowest fibril/cholesterol binding energy in all lipid rafts.

For the case of GM-raft, the fibril/GM1 binding energies ranged from~ −600 to −1600 kJ/mol when the fibril directly associated with the GM1 headgroups, as shown in Fig. S17E. [26] The lowest fibril/GM1 energy was found in the GM-ABCD-2 (L-state), and the highest in the GM-AB-2 (S-state). For two simulation replicates, GM-AB-3 (C-state) and GM-ABCDE-2 (C-state), did not bind to GM1, showing zero fibril/GM1 binding energy as expected. The L-state had the highest binding energy among all replicates showing direct GM1 binding. Also, the replicate that did not bound to GM1, i.e., AB-3 or ABCDE-2, had significantly higher total fibril/lipid binding energy compared to the replicates of the same fibril size but bound to GM1.

Since the binding energies of the fibril and lipids depend on the number of lipids surrounding the fibril, we also calculated a binding energy per lipid, defined as the binding

Author Manuscript Author Manuscript Author Manuscript Author Manuscript

energy divided by the number of lipids with a fibril-lipid minimum-distance of 1 nm, or the total lipids within the first two annular lipid shells. The choice of a 1 nm cutoff is based on the cutoff of long-range interactions being set at 1.2 nm (see Methods). Note that the 0.5–1 nm annular lipid shell was determined based on the minimum distance between the atoms of fibril and lipids, and some of the atoms within the lipid shells are greater than 1 nm. The normalized binding energy, or binding energy per lipid, is shown in Fig.S30 [26].

3.4. Structure and composition of annular lipid shells

To identify the lateral extent of fibril induced perturbation of the lipid bilayer in the local vicinity of the bound fibril and beyond, the composition and structure of lipid molecules surrounding the membrane-bound fibril, or annular lipid shells, were examined. These lipid shells were determined based on the distances between the atoms of the membrane-bound fibril and lipids that satisfy the following criteria, less than 5 Å (shell 1), 5 to 10 Å (shell 2), 10 to 20 Å (shell 3) and 20 to 30 Å (shell), as discussed in Methods. Fig. S32 [26] demonstrates the lipids belonging to each shell in both lateral and transverse views of a dimer bound to the CO-raft. It is clear that the first two annular lipid shells (Figs. S32A and B [26]) include lipids in only one monolayer. However, the last two, or larger annular shells (Figs. S32 C and D [26]) included lipids from both monolayers.

Analysis of the annular lipid shells around the beta-amyloid fibrils for all rafts confirms that fibrils prefer to bind the Lod domain, with fibrils preferentially binding to GM1-clusters in GM1-containing rafts. The lipid composition of the annular lipid shells of all simulation replicates are shown in Fig. S33 [26]. For the non-GM-rafts, CHOL or modified CHOL accounted for ~20–30%, DPPC ~ 20–40%, and DLPC ~ 10–30%, indicating the preference of fibril binding to lipids in the Lod domain rather than the Lo or Ld domains. Note that significantly lower C1-CHOL% in the first lipid shell was observed for the T- and N-state, compared with the higher order lipid shells. For the GM-raft, the larger GM1% was found in the first lipid shell and this percentage decreased dramatically in the higher order lipid shells. As expected, the GM1% was zero for the first lipid shell for the AB-2 or ABCD-2 replicates where the fibril bound to the monolayer without GM1.

The transverse distributions, number density vs z distance, of the DPPC headgroup (PO4) and cholesterol headgroup (ROH) in each lipid shell for different membrane-bound states were examined as demonstrated in Fig. S34 [26]. In general, the peak of the PO4 headgroup of DPPC in the first and second shells slightly shifted (< 0.5 nm) towards the right, where the fibril was located, when compared with those in the third and fourth shells for the C-, N-, -T and I-states. Similarly, the peak of the ROH headgroup of CHOL in the first and second shells also slightly shifted towards the right for both the C- and T-state of the CO-raft. However, a larger shift (> 1nm) of the ROH headgroup of C1-CHOL was evident for the C- and N-states of the C1-raft. In contrast, no significant shift in the ROH headgroup of P1-CHOL of the P1-raft was observed. Again, a single ROH peak for the C1-raft (Figs. S34C and D [26]) and a trimodal ROH peak for the P1-raft (Figs. 34E and F [26]) in the last two lipid shells were detected, and the results agreed with the observations of ROH peaks in Lo, Ld and Lod domains for the same lipid raft. Similar observations of transverse distribution of lipids in P4- and GM-rafts are given in Fig. S35. [26]

Author Manuscript Author Manuscript Author Manuscript Author Manuscript

The order parameters of DPPC, DLPC and cholesterol (or modified cholesterol) in non-GM1 containing rafts in all simulation replicates were calculated as shown in Figs. S36 [26]. In general, the lipid order parameter in the first shell was low but increased progressively in higher order lipid shells, except for the P1-ABC-2 replicate in the I-state. The order parameter of C1-CHOL in the C1-raft was lowest when compared with CHOL or other modified CHO in other rafts. For the first annular lipid shell, the DPPC and CHOL order parameters were significantly lower for the larger fibrils than those for the smaller fibrils, particularly for the P1-raft, e.g., the P1-CHOL order parameter was 0.2–0.4 for the dimer but dropped to −0.1 to 0.1 for the pentamer. Similar observation of the fibril size effects was found for the GM1-raft. Due to the large fluctuation in the fibril-lipid contacts, as shown in the number of contacts vs. time plots in Figs. 8 and 10, the time-averaged lipid order parameter has large uncertainty. Figs. S37–40 [26] show large fluctuation in the lipid order parameter as a function of time in different annular lipid shells.

4. Discussion

Using CG lipids, five lipid rafts: CO-raft, C1-raft, P1-raft, P4-raft and GM-raft, with phase-separated lipid domains of varying domain structures have successfully been created. Ordered DPPC-rich (Lo), disordered DLPC-rich (Ld), and mixed DPPC-DLPC (Lod) domains were observed in all rafts. Compositional and lipid chain orientational analysis of the rafts revealed remarkable structural stability of these domains without fibrils and in the presence of fibrils, throughout the entire 20 μs MD simulations. Therefore, these lipid raft systems are useful computational models that mimic the complex, highly dynamic, and compositionally and structurally diversified domain structures found in cell membranes.[14, 42]

The use of modified CHOL, i.e., C1-CHOL, P1-CHOL or P4-CHOL, allows us to modify or control the domain structure of the lipid raft systematically. Here, the amount or fraction of Lod in each lipid raft decreases in the following order: C1-raft, P1-raft, GM-raft, CO-raft and P4-raft. This variation of Lod fraction is associated with the hydrophobicity of the cholesterol, as hydrophobic C1-CHOL disrupts the Lo and Ld domains while enhancing the Lod domain. On the other hand, the more hydrophilic P4-CHOL increases the size of Lo and Ld domains but decreases the Lod domain. The domain modulation effects of cholesterol are mainly associated with their partitioning behavior within the lipid bilayer of the membrane.[17] Our orientational order and the transverse density profile calculations indicate that C1-CHOL and P1-CHOL can dive into the center of the bilayer, while P4-CHOL is mainly aligned with the bilayer normal. The presence of GM1 does not significantly perturb the domain structure found in CO-CHOL raft. Yet, GM1 aggregates and partitions exclusively in the Lo domain confirming the role of GM1 as the major lipid marker of lipid rafts in cell membranes. The asymmetric distribution of GM1 in GM-raft was maintained over the entire 20 μs simulation indicating the validity of our four-component lipid raft in modeling the raft structure in cell membranes.[43, 44] Finally, the asymmetric GM1 clusters allows us to compare fibril/lipid binding behaviors in model asymmetric membranes with and without receptors.

Author Manuscript Author Manuscript Author Manuscript Author Manuscript

Our results indicate that oxysterols can modulate the domain structures of the raft systems. We suggest that the presence of cholestenone or 27-hydroxycholesterol, as modeled by C1-CHOL or P1-CHOL, enhance the Lod domain, while 5-alpha-hydroxycholesterol, as modeled by P4-CHOL, enhance the Lo and Ld domains. This predicted lipid domain modulation effects of oxysterol remain to be confirmed by experiments.

Diverse membrane-bound states of fibrils of different sizes on raft membrane surfaces have been systematically studied for the non-GM1 containing rafts and GM1-rafts. Our results clearly establish that the binding of dimer fibril involves interactions between the protein C-terminal and the lipid headgroups, or the C-state, in all non-GM1 rafts. This observation suggests that interaction between the hydrophobic C-terminal region of the dimer and the Lod domain of the phase-separated membrane represent the prevalent dimer-membrane binding mechanism in lipid rafts without receptor, such as GM1-clusters in the GM-raft.

On the other hand, in the presence of GM1 cluster in GM-raft, both the hydrophilic N-terminal and hydrophobic C-terminal regions of dimer bound to the membrane surface to form the S-state in two out of three simulation replicates. Here, in this S-state, the dimer residues were closely associated with the highly hydrophilic GM1 headgroup consisting of carbohydrate residues that facilitate the N-terminal binding. Interestingly, for the third replicate which did not bind to the GM1-containing lipid monolayer, the C-state was again detected, and further supports the prevalent C-terminal binding behavior of dimer to membrane surface with no GM1-receptors as observed in non-GM1-containing rafts.

For larger fibrils, diversified membrane-bound states, T-, N- and I-states for non-GM1 containing rafts, and N- and I states for the GM-raft, in addition to the C-state were observed. For the non-GM1 containing rafts, the T-state and N-state, had lower binding energy to the lipids than the C-state for the same fibril size in each raft system, except the N-state of the P1-raft. These results indicate that these non-C-states were loosely bound to the lipid headgroup since both T- and N-regions of the fibril contains hydrophilic residues that did not bind strongly to the non-GM1 lipid headgroups. The I-state is the only transmembrane protein inserted state that we have found in all 60 fibril/raft simulation systems that we investigated. In this state, a stable inserted trimer fibril in P1-raft was detected. The highest protein/cholesterol binding energy was detected. The presence of the transmembrane protein inserted state in the P1-raft suggests that the beta-amyloid fibril, trimer in our case, can insert into the lipid bilayer via the Lod domain from the solution phase. The results further indicate the diversity of different membrane-bound states of fibrils and the binding affinity of fibrils from strong bound states, such as inserted I-state and surface C-state, to weak bound states, such as all T-state and N-state, in lipid rafts.

Our results suggest that while the rare states (N-State, T-State, L-State, and I-State) may not occur as often, when then do, they can interact strongly with the lipid rafts (especially in rafts containing modified cholesterol or GM1). Targeting these rare, but strongly interacting states, could provide a new avenue for drug discovery and design for future therapeutic interventions for Alzheimer’s.

Author Manuscript Author Manuscript Author Manuscript Author Manuscript

Our results of exclusive binding of beta-amyloid fibrils of all sizes to Lod domain in non-GM1-rafts agree with an experimental observation of HIV-gp41 fusion peptide binding to the Lod domain boundaries.[45] The line tension created at the domain boundaries due to the hydrophobic mismatch between the thicker and order Lo domain and the thinner and disordered Ld domain has been identified as the mechanism driving the protein binding for the case of HIV-gp4 [45, 46]. Similar mechanisms may also be responsible for our observations of fibril binding to Lod in our highly diversified rafts.

For the GM1-containing rafts, strong binding among fibrils to GM1 headgroups was found for all fibril sizes, except a dimer and a pentamer, which bound to the non-GM1-containing monolayer in GM-raft involving the C-state, similar to the non-GM1 binding events described above. However, low protein/lipid energy binding was found in the L-state, in which only the fibril loop interacted with the GM1. Since the surface area of the loop is considerably smaller than that of the C- or N-terminal, the low protein/lipid binding energy of L-state is not surprising. Our results also suggest that the GM1-headgroup acts as a receptor to attract the beta-amyloid fibrils from the solution phase to form beta-amyloid/GM1 complexes of different membrane-bound states in the GM1-raft. These initial binding events, as captured in this simulation study, may lead to further structural disruption or even detergent-like effect, on lipid membranes, as demonstrated in recent experimental studies.[47–49]

In all-atom simulations, the electrostatic or coulomb interactions are major interactions, and they arise due to partial charges distributed among the atoms [50, 51]. In Martini CG force fields [28, 30], a pseudo or CG atom represents ~ 4 heavy atoms. As a result, the charge assignment in CG force fields is different from all-atom force fields, e.g., CG-CHOL has no charge, but CHOL has partial charge in non-CG force fields. The same applies to lipid headgroup and amino acid residues. Here each DPPC or DLPC has a +1 charge of PO4 and −1 charge of NC3, while the charged amino acid has either −1 or +1 charge in the side chain but no charge in the backbone. The GM1 has a single −1 charge and the C-terminus has a single −1 charge. Due to the differences in parameterization of different atomic force fields, partial charge assignments will vary, so while insight about the nature of binding can be gained from all-atom simulations, they cannot be directly extrapolated to interpret coarse-grained results. Additionally, all-atom results suffer from limited simulation times, whereas CG simulations provide more efficient sampling, allowing us to explore the energy landscape and diverse binding-states of fibrils to complex multicomponent lipid rafts at biologically relevant time scales.

The two major interactions in Martini CG force fields are the Lennard-Jones (LJ) and Coulomb (Coul) interactions. We have looked into the Coul/LJ binding energy ratio in all of our calculations. The results are shown in Figure S31. This ratio is always lower than 0.20. However, we seem to identify a trend that this ratio is higher in the T or N state than in the C state for the non-GM1 rafts, with the exception of the N-state in P1-raft. Therefore, the electrostatic interaction is stronger in the N or T-state than in the C-state for CO-raft, C1-raft and P4-raft. The S-state of GM1 has the strongest Coulomb interaction with the lipids than any other states

Author Manuscript Author Manuscript Author Manuscript Author Manuscript

The two major interactions in Martini CG force fields are the Lennard-Jones (LJ) and Coulomb (Coul) interactions. We have looked into the Coul/LJ binding energy ratio in all of our calculations. The results are shown in Figure S31. This ratio is always lower than 0.20. However, we seem to identify a trend that this ratio is higher in the T or N state than in the C state for the non-GM1 rafts, with the exception of the N-state in P1-raft. Therefore, the electrostatic interaction is stronger in the N or T-state than in the C-state for CO-raft, C1-raft and P4-raft. The S-state of GM1 has the strongest Coulomb interaction with the lipids than any other states

It is important to mention that fibril/membranes have been investigated extensively by experimental and computational methods [39, 50–59]. Various predictions have been proposed regarding the binding domain of fibrils and the orientational order of protein. In one recent all-atom simulation work [50], the authors used the same amyloid fibrils as in this work and observed stabilized C-state and I-state in a pure DOPC bilayer within 500 ns all-atom simulations. The observed membrane-bound orientations from their all-atom simulations are similar to those predicted by our CG-simulations. Note, that instead of using pre-assembled protein/lipid complexes as the initial states as in most all-atom simulations, we observed binding from protein-in-solution state, anchored protein-to-membrane surface state, then to equilibrated membrane-bound state via lateral motion of the fibril on membrane surface in our CG-simulation study. Therefore, our system sampled extensive rotational and translational states in both solution and membrane-bound environment. However, our CG-system fails to provide detailed and important atomistic interactions of fibril and lipids, as all-atom studies provide. [50] We believe that our CG-study validates and supplements the important finding of the above all-atom work which focused on two amyloid fibrils in a pure PC bilayer. Our study provides new information on the long microsecond sampling time and multi-component raft-like lipid bilayers with phase separations.

A concern is raised about the Lod phase preference of fibril binding to lipid rafts. The relative surface area of Lod is as high as ~ 90% in C1-raft to ~ 60% in CO-raft or P4-raft (Figure S3A). Since the Lod is larger in surface area than the other phases, it is reasonable that the fibril first lands on the Lod phase from the solution phase, before establishing a stable membrane-bound state. However, the fibril undergoes lateral movement on the surface of the bilayer, and the fibril is able to sample other phases before establishing a final equilibrated membrane-bound state.

We further address the Lod phase-preference concern by determining the residence time of fibril in each phase, i.e., Lo-residence time, Ld-residence time and Lod-residence time, based on the minimum-distance vs. time data (upper panel of each plot in Figs 8, 9, S17–21 [26]). Here, the Lo- or Ld-residence time was calculated by enumerating the times that the minimum distance between the atoms of fibril and DLPC or DPPC molecules are greater than the threshold of 0.5 nm, respectively. Upon dividing the Lo- or Ld-residence time by the total amount of time the fibril stayed on membrane, the Lo- or Ld-residence time % was then determined. The Lod-residence time % is (100 - Lo-residence time % - Ld-residence time %). The results of the phase-residence time for all rafts are shown in Figure S22 [26]. It is evident that upon binding to lipid membrane, the fibrils did sample other phases, mostly

Author Manuscript Author Manuscript Author Manuscript Author Manuscript

Lo. For the CO-raft and P4-raft with only ~ 30% surface area, some fibrils exhibited a significant Lo-residence time up to ~20%. Since Ld accounts for less than 10% surface area, no significant Ld-residence time (< 5%) was observed. We believe that future work is still needed to confirm the Lod phase preference by simulating rafts with wider ranges of surface area of each phase.

Our microsecond simulated binding conformation and energetics in our model coarse-grained fibril/raft complexes may provide useful insights in understanding regulatory roles of lipid domains in the binding of beta-sheet enriched fibrils to heterogeneous lipid domains in cell membranes. This study provides useful information for future atomistic simulation study to reveal finer binding conformation and protein-folding and unfolding on membrane surface. In addition, the membrane-bound conformational information is useful for future drug-intervention targeting aggregated amyloidogenic protein bound to lipid membranes at the early stage of fibril/membrane interactions.

5. Conclusion

Using CG MD simulations, the binding kinetics and membrane-bound conformations of beta-amyloid fibrils on the surface of phase-separated lipid rafts were examined. Within 20 μs, all fibrils bound to Lod domains of non-GM1-containing rafts, exhibiting diverse membrane-bound states. Dimer fibrils bound exclusively via the C-state, whereas larger fibrils bound weakly via N- and T-states. Only one inserted state, I-state, was detected in the P1-raft with the trimer fibril. In this I-state, the trimer fibril directly inserted into the P1-raft from solution state to a transmembrane state. For the GM1-containing rafts, the fibrils attached to the surface GM1-cluster and exhibited diversified C-, N-, S- and L- states. Interestingly, non-specific GM1 binding in GM-raft, i.e., binding of a dimer and a pentamer fibril to the Lod domain via the C-terminal (C-state) was revealed. We propose that the observed fibril binding to the Lod domains in the non-GM1-rafts and the diverse membrane conformations observed in non-GM1- and GM1-rafts may also be operative in structurally heterogeneous cell membranes. Understanding the binding preferences of beta-amyloid fibrils to the Lod domains and GM1-clusters and the membrane-bound conformations may be useful for developing drugs to inhibit the binding of beta-amyloid fibrils to specific lipid domains, allowing for therapeutic intervention at the early stages of Alzheimer’s pathogenesis.

Supplementary Material

Refer to Web version on PubMed Central for supplementary material.

Acknowledgements

We thank Donald Davenport-Deny, Alejandro G. Urby and Sophia Spurlock for their help in the design and simulations of some early versions of fibril and rafts.

8. Funding Sources

Supported by the Robert A. Welch Foundation [D-1158], National Science Foundation [OAC 153159], National Institutes of Health [RC1GM090897], and Howard Hughes Medical Institute Undergraduate Fellowship.

Author Manuscript Author Manuscript Author Manuscript Author Manuscript

10. References

[1]. Luhrs T, Ritter C, Adrian M, Riek-Loher D, Bohrmann B, Dobeli H, Schubert D, Riek R, 3D structure of Alzheimer's amyloid-beta(1–42) fibrils, Proc Natl Acad Sci U S A, 102 (2005) 17342–17347. [PubMed: 16293696]

[2]. Shea D, Hsu CC, Bi TM, Paranjapye N, Childers MC, Cochran J, Tomberlin CP, Wang L, Paris D, Zonderman J, Varani G, Link CD, Mullan M, Daggett V, alpha-Sheet secondary structure in amyloid beta-peptide drives aggregation and toxicity in Alzheimer's disease, Proc Natl Acad Sci U S A, 116 (2019) 8895–8900. [PubMed: 31004062]

[3]. Sahoo A, Xu H, Matysiak S, Pathways of amyloid-beta absorption and aggregation in a membranous environment, Physical Chemistry Chemical Physics, 21 (2019) 8559–8568. [PubMed: 30964132]

[4]. Zhang X, Fu Z, Meng L, He M, Zhang Z, The Early Events That Initiate beta-Amyloid Aggregation in Alzheimer's Disease, Front Aging Neurosci, 10 (2018) 359. [PubMed: 30542277]

[5]. Li H, Liu C-C, Zheng H, Huang TY, Amyloid, tau, pathogen infection and antimicrobial protection in Alzheimer's disease –conformist, nonconformist, and realistic prospects for AD pathogenesis, Translational Neurodegeneration, 7 (2018) 34. [PubMed: 30603085]

[6]. Selkoe DJ, Hardy J, The amyloid hypothesis of Alzheimer's disease at 25 years, EMBO Mol Med, 8 (2016) 595–608. [PubMed: 27025652]

[7]. Corradi V, Sejdiu BI, Mesa-Galloso H, Abdizadeh H, Noskov SY, Marrink SJ, Tieleman DP, Emerging Diversity in Lipid-Protein Interactions, Chem Rev, 119 (2019) 5775–5848. [PubMed: 30758191]

[8]. Egawa J, Pearn ML, Lemkuil BP, Patel PM, Head BP, Membrane lipid rafts and neurobiology: age-related changes in membrane lipids and loss of neuronal function, J Physiol, 594 (2016) 4565–4579. [PubMed: 26332795]

[9]. Martin MG, Pfrieger F, Dotti CG, Cholesterol in brain disease: sometimes determinant and frequently implicated, EMBO Rep, 15 (2014) 1036–1052. [PubMed: 25223281]

[10]. Pfrieger FW, Ungerer N, Cholesterol metabolism in neurons and astrocytes, Prog Lipid Res, 50 (2011) 357–371. [PubMed: 21741992]

[11]. Butterfield DA, Abdul HM, Lipids in Alzheimer's Disease Brain, in: Lajtha A, Tettamanti G, Goracci G (Eds.) Handbook of Neurochemistry and Molecular Neurobiology: Neural Lipids, Springer US, Boston, MA, 2009, pp. 563–582.

[12]. Julian MC, Rabia LA, Desai AA, Arsiwala A, Gerson JE, Paulson HL, Kane RS, Tessier PM, Nature-inspired design and evolution of anti-amyloid antibodies, J Biol Chem, 294 (2019) 8438–8451. [PubMed: 30918024]

[13]. Grasso G, Rebella M, Morbiducci U, Tuszynski JA, Danani A, Deriu MA, The Role of Structural Polymorphism in Driving the Mechanical Performance of the Alzheimer's Beta Amyloid Fibrils, Front Bioeng Biotechnol, 7 (2019) 83. [PubMed: 31106199]

[14]. Marrink SJ, Corradi V, Souza PCT, Ingolfsson HI, Tieleman DP, Sansom MSP, Computational Modeling of Realistic Cell Membranes, Chem Rev, 119 (2019) 6184–6226. [PubMed: 30623647]

[15]. Bennett WF, Tieleman DP, Computer simulations of lipid membrane domains, Biochim Biophys Acta, 1828 (2013) 1765–1776. [PubMed: 23500617]

[16]. Bennett WFD, Shea JE, Tieleman DP, Phospholipid Chain Interactions with Cholesterol Drive Domain Formation in Lipid Membranes, Biophys J, 114 (2018) 2595–2605. [PubMed: 29874610]

[17]. Perlmutter JD, Sachs JN, Inhibiting lateral domain formation in lipid bilayers: simulations of alternative steroid headgroup chemistries, J Am Chem Soc, 131 (2009) 16362–16363. [PubMed: 19860442]

[18]. Axelsen PH, Komatsu H, Murray IV, Oxidative stress and cell membranes in the pathogenesis of Alzheimer's disease, Physiology (Bethesda), 26 (2011) 54–69. [PubMed: 21357903]

[19]. Griffiths WJ, Wang Y, Oxysterol research: a brief review, Biochem Soc Trans, 47 (2019) 517–526. [PubMed: 30936243]

Author Manuscript Author Manuscript Author Manuscript Author Manuscript

[20]. Masters CL, Cappai R, Barnham KJ, Villemagne VL, Molecular mechanisms for Alzheimer's disease: implications for neuroimaging and therapeutics, J Neurochem, 97 (2006) 1700–1725. [PubMed: 16805778]

[21]. Phan HT, Hata T, Morita M, Yoda T, Hamada T, Vestergaard MC, Takagi M, The effect of oxysterols on the interaction of Alzheimer's amyloid beta with model membranes, Biochim Biophys Acta, 1828 (2013) 2487–2495. [PubMed: 23800382]

[22]. Tonnies E, Trushina E, Oxidative Stress, Synaptic Dysfunction, and Alzheimer's Disease, J Alzheimers Dis, 57 (2017) 1105–1121. [PubMed: 28059794]

[23]. Risselada HJ, Marrink SJ, The molecular face of lipid rafts in model membranes, Proc Natl Acad Sci U S A, 105 (2008) 17367–17372. [PubMed: 18987307]

[24]. Róg T, Vattulainen I, Cholesterol, sphingolipids, and glycolipids: What do we know about their role in raft-like membranes?, Chemistry and Physics of Lipids, 184 (2014) 82–104. [PubMed: 25444976]

[25]. Faridi A, Yang W, Kelly HG, Wang C, Faridi P, Purcell AW, Davis TP, Chen P, Kent SJ, Ke PC, Differential Roles of Plasma Protein Corona on Immune Cell Association and Cytokine Secretion of Oligomeric and Fibrillar Beta-Amyloid, Biomacromolecules, 20 (2019) 4208–4217. [PubMed: 31600059]

[26]. Cheng SY, Cao Y, Rouzbehani M, Cheng KH, Data Showing the Lipid Conformations and Membrane Binding Behaviors of Beta-Amyloid Fibrils in Phase-Separated Cholesterol-Enriched Lipid Domains With and Without Glycolipid and Oxidized Cholesterol from Coarse-Grained Molecular Dynamics Simulations, Data in Brief, (pending) (2020).

[27]. Marrink SJ, de Vries AH, Mark AE, Coarse Grained Model for Semiquantitative Lipid Simulations, J Phys Chem B, 108 (2004) 750–760.

[28]. Marrink SJ, Risselada HJ, Yefimov S, Tieleman DP, de Vries AH, The MARTINI force field: coarse grained model for biomolecular simulations, J Phys Chem B, 111 (2007) 7812–7824. [PubMed: 17569554]

[29]. de Jong DH, Singh G, Bennett WF, Arnarez C, Wassenaar TA, Schafer LV, Periole X, Tieleman DP, Marrink SJ, Improved Parameters for the Martini Coarse-Grained Protein Force Field, J Chem Theory Comput, 9 (2013) 687–697. [PubMed: 26589065]

[30]. Monticelli L, Kandasamy SK, Periole X, Larson RG, Tieleman DP, Marrink SJ, The MARTINI Coarse-Grained Force Field: Extension to Proteins, J Chem Theory Comput, 4 (2008) 819–834. [PubMed: 26621095]

[31]. Periole X, Cavalli M, Marrink SJ, Ceruso MA, Combining an Elastic Network With a Coarse-Grained Molecular Force Field: Structure, Dynamics, and Intermolecular Recognition, J Chem Theory Comput, 5 (2009) 2531–2543. [PubMed: 26616630]

[32]. Hess B, Kutzner C, van der Spoel D, Lindahl E, GROMACS 4: Algorithms for Highly Efficient, Load-Balanced, and Scalable Molecular Simulation, J Chem Theory Comput, 4 (2008) 435–447. [PubMed: 26620784]

[33]. Hess B, Bekker H, Berendsen HJC, Fraaije JGEM, LINCS: A linear constraint solver for molecular simulations, Journal of Computational Chemistry, 18 (1997) 1463–1472.

[34]. Essmann U, Perera L, Berkowitz ML, Darden T, Lee H, Pedersen LG, A smooth particle mesh Ewald method, The Journal of Chemical Physics, 103 (1995) 8577–8593.

[35]. Berendsen HJC, Postma JPM, van Gunsteren WF, DiNola A, Haak JR, Molecular dynamics with coupling to an external bath, J Chem Phys, 81 (1984) 3684–3690.

[36]. Bussi G, Donadio D, Parrinello M, Canonical sampling through velocity rescaling, The Journal of Chemical Physics, 126 (2007) 014101. [PubMed: 17212484]

[37]. Hockney RW, Goel SP, Eastwood JW, Quiet high resolution computer models of a plasma, Journal of Computational Physics, 14 (1974) 148–158.

[38]. Cheng SY, Chou G, Buie C, Vaughn MW, Compton C, Cheng KH, Maximally asymmetric transbilayer distribution of anionic lipids alters the structure and interaction with lipids of an amyloidogenic protein dimer bound to the membrane surface, Chem Phys Lipids, 196 (2016) 33–51. [PubMed: 26827904]

[39]. Allen WJ, Lemkul JA, Bevan DR, GridMAT-MD: a grid-based membrane analysis tool for use with molecular dynamics, J Comput Chem, 30 (2009) 1952–1958. [PubMed: 19090582]

Author Manuscript Author Manuscript Author Manuscript Author Manuscript

[40]. Ali MR, Cheng KH, Huang J, Assess the nature of cholesterol-lipid interactions through the chemical potential of cholesterol in phosphatidylcholine bilayers, Proc Natl Acad Sci U S A, 104 (2007) 5372–5377. [PubMed: 17372226]

[41]. Humphrey W, Dalke A, Schulten K, VMD: visual molecular dynamics, J Mol Graph, 14 (1996) 33–38, 27–38. [PubMed: 8744570]

[42]. Raghunathan K, Kenworthy AK, Dynamic pattern generation in cell membranes: Current insights into membrane organization, Biochim Biophys Acta Biomembr, 1860 (2018) 2018–2031. [PubMed: 29752898]

[43]. Yu RK, Tsai YT, Ariga T, Functional roles of gangliosides in neurodevelopment: an overview of recent advances, Neurochem Res, 37 (2012) 1230–1244. [PubMed: 22410735]

[44]. Yamakawa T, Nagai Y, Glycolipids at the cell surface and their biological functions, Trends in Biochemical Sciences, 3 (1978) 128–131.

[45]. Yang S-T, Kiessling V, Tamm LK, Line tension at lipid phase boundaries as driving force for HIV fusion peptide-mediated fusion, Nature Communications, 7 (2016) 11401.

[46]. Akimov SA, Kuzmin PI, Zimmerberg J, Cohen FS, Lateral tension increases the line tension between two domains in a lipid bilayer membrane, Phys Rev E Stat Nonlin Soft Matter Phys, 75 (2007) 011919. [PubMed: 17358196]

[47]. Rushworth JV, Hooper NM, Lipid Rafts: Linking Alzheimer's Amyloid-beta-Production, Aggregation, and Toxicity at Neuronal Membranes, International Journal of Alzheimer's Disease, 2011 (2011).

[48]. Kandel N, Matos JO, Tatulian SA, Structure of amyloid beta25–35 in lipid environment and cholesterol-dependent membrane pore formation, Sci Rep, 9 (2019) 2689. [PubMed: 30804528]

[49]. Bode DC, Freeley M, Nield J, Palma M, Viles JH, Amyloid-beta oligomers have a profound detergent-like effect on lipid membrane bilayers, imaged by atomic force and electron microscopy, J Biol Chem, 294 (2019) 7566–7572. [PubMed: 30948512]

[50]. Jang H, Connelly L, Arce FT, Ramachandran S, Kagan BL, Lal R, Nussinov R, Mechanisms for the Insertion of Toxic, Fibril-like beta-Amyloid Oligomers into the Membrane, J Chem Theory Comput, 9 (2013) 822–833. [PubMed: 23316126]

[51]. Carballo-Pacheco M, Ismail AE, Strodel B, On the Applicability of Force Fields To Study the Aggregation of Amyloidogenic Peptides Using Molecular Dynamics Simulations, J Chem Theory Comput, 14 (2018) 6063–6075. [PubMed: 30336669]

[52]. Tachi Y, Okamoto Y, Okumura H, Conformational Change of Amyloid-beta 40 in Association with Binding to GM1-Glycan Cluster, Sci Rep, 9 (2019) 6853. [PubMed: 31048748]

[53]. Press-Sandler O, Miller Y, Molecular mechanisms of membrane-associated amyloid aggregation: Computational perspective and challenges, Biochim Biophys Acta Biomembr, (2018).

[54]. Brown AM, Bevan DR, Molecular Dynamics Simulations of Amyloid beta-Peptide (1–42): Tetramer Formation and Membrane Interactions, Biophys J, 111 (2016) 937–949. [PubMed: 27602722]

[55]. Bucciantini M, Nosi D, Forzan M, Russo E, Calamai M, Pieri L, Formigli L, Quercioli F, Soria S, Pavone F, Savistchenko J, Melki R, Stefani M, Toxic effects of amyloid fibrils on cell membranes: the importance of ganglioside GM1, FASEB J, 26 (2012) 818–831. [PubMed: 22071505]

[56]. Sengupta U, Carballo-Pacheco M, Strodel B, Automated Markov state models for molecular dynamics simulations of aggregation and self-assembly, J Chem Phys, 150 (2019) 115101. [PubMed: 30901988]

[57]. Poojari C, Strodel B, Stability of transmembrane amyloid beta-peptide and membrane integrity tested by molecular modeling of site-specific Abeta42 mutations, PLoS One, 8 (2013) e78399. [PubMed: 24244308]

[58]. Carballo-Pacheco M, Strodel B, Advances in the Simulation of Protein Aggregation at the Atomistic Scale, J Phys Chem B, 120 (2016) 2991–2999. [PubMed: 26965454]

[59]. Nasica-Labouze J, Nguyen PH, Sterpone F, Berthoumieu O, Buchete NV, Cote S, De Simone A, Doig AJ, Faller P, Garcia A, Laio A, Li MS, Melchionna S, Mousseau N, Mu Y, Paravastu A, Pasquali S, Rosenman DJ, Strodel B, Tarus B, Viles JH, Zhang T, Wang C, Derreumaux P,

Author Manuscript Author Manuscript Author Manuscript Author Manuscript

Amyloid beta Protein and Alzheimer's Disease: When Computer Simulations Complement Experimental Studies, Chem Rev, 115 (2015) 3518–3563. [PubMed: 25789869]

Author Manuscript Author Manuscript Author Manuscript Author Manuscript

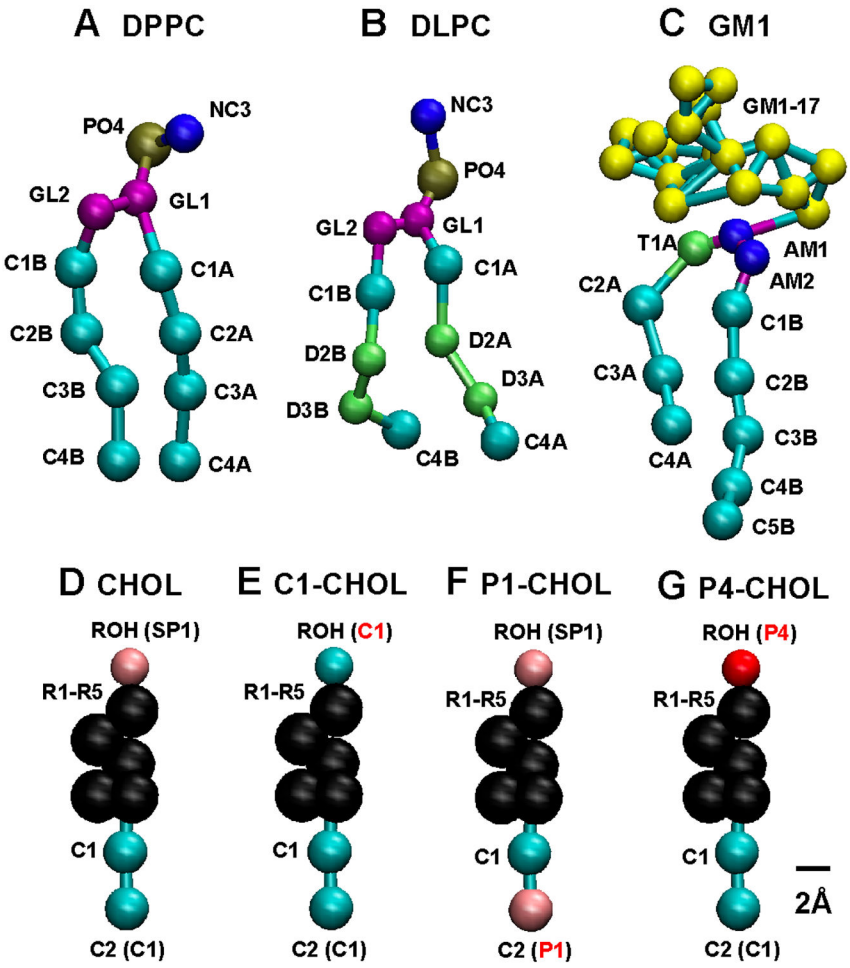

Figure 1.

Coarse-grained (CG) structure of DPPC (A), DLPC (B), GM1 (C), CHOL (D), and modified CHO: C1-CHOL (E), P1-CHOL (F) and P4-CHOL (G), in colored beads and rods, with the CG-atom labels identified. To create modified CHO (E-G), the atom type given in parenthesis for the headgroup ROH of CHO is modified from SP1 (D) to C1 (E) or P4 (G) in red, and that for the tail group C2 of CHO from C1 (D) to P1 (F) in red. A scale bar of 2 Å is shown.

Author Manuscript Author Manuscript Author Manuscript Author Manuscript

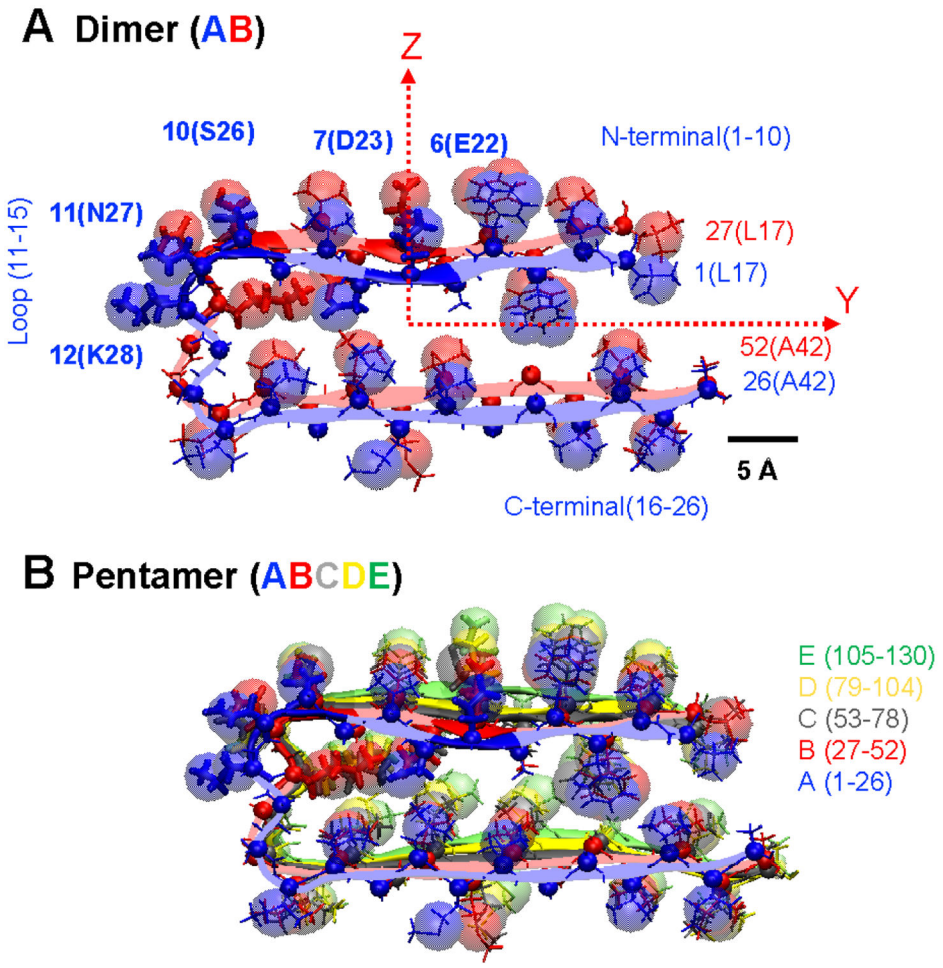

Figure 2.

Initial structure of beta-amyloid fibrils $(A\beta_{17–42})_n$ of n = 2 or dimer (A) and of n = 5 or pentamer (B). Fibril chains A, B, C, D and E are labeled by blue, red, gray, yellow and green, respectively, for coarse-grained (CG) in color beads and atomistic in ribbon and lines structures. Marked in bold, the five polar amino acid residues: E22, D23, S26 along the N-terminal, N27 and K28 along the loop, and their corresponding residue locations: 6, 7, 10, 11 and 12, are illustrated for chain A. For clarity, the residue locations of our CG fibril chains are labeled as 1–26, 27–52, 53–78, 79–104 and 105–130 for chains A, B, C, D and E, accordingly (B). The molecular axes (X-Y-Z) were determined from the calculated moment of inertia principal axes such that the Z-principal axis is along the beta-sheet direction of the fibril. The Y and Z molecular axes, marked in red, of the dimer fibril (A) are shown. A scale bar of 5 Å is also given.

Author Manuscript Author Manuscript Author Manuscript Author Manuscript

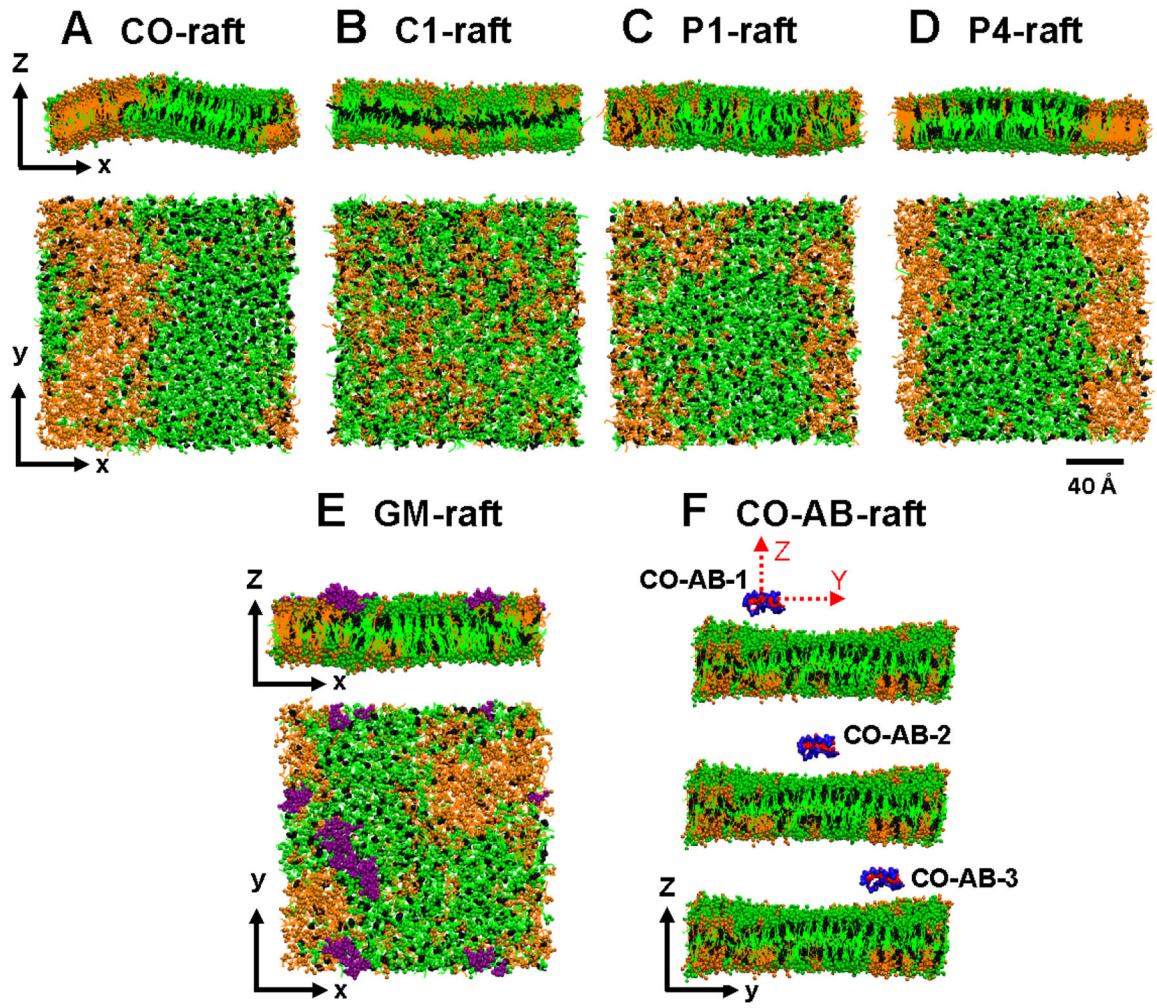

Figure 3.

The initial coarse-grained (CG) structures of CO-raft (A), C1-raft (B), P1-raft (C), P4-raft (D), and GM-raft (E), with their constituent lipids, DPPC (green), DLPC (orange), cholesterol or modified cholesterol (black) and GM1 (purple). The (x, y, z) coordinate system of the simulation box with z along the normal or the transverse direction of the lipid bilayer is used. Here, the transverse, (x, z) or (y, z), and lateral (x, y), planes are identified. DPPC, DLPC and CHO headgroups, as well as the ring groups of CHO, are rendered in spheres, whereas the acyl tails of phospholipid and cholesterol are in thin lines. For creating the initial fibril/raft simulation replicates, the center of mass of each fibril was placed at (0, −5nm, 5nm), (0, 0, 5nm) or (0, 5nm, 5nm), all in nm, with respect to the center (0, 0, 0) of each lipid raft. The three simulation replicates for the CO-AB complex are identified as CO-AB-1, CO-AB-2 and CO-AB-3 (F). The alignment of the molecular axes (Y-Z) with the simulation box axis (y-z) is demonstrated. A scale bar of 40 Å is given.

Author Manuscript Author Manuscript Author Manuscript Author Manuscript

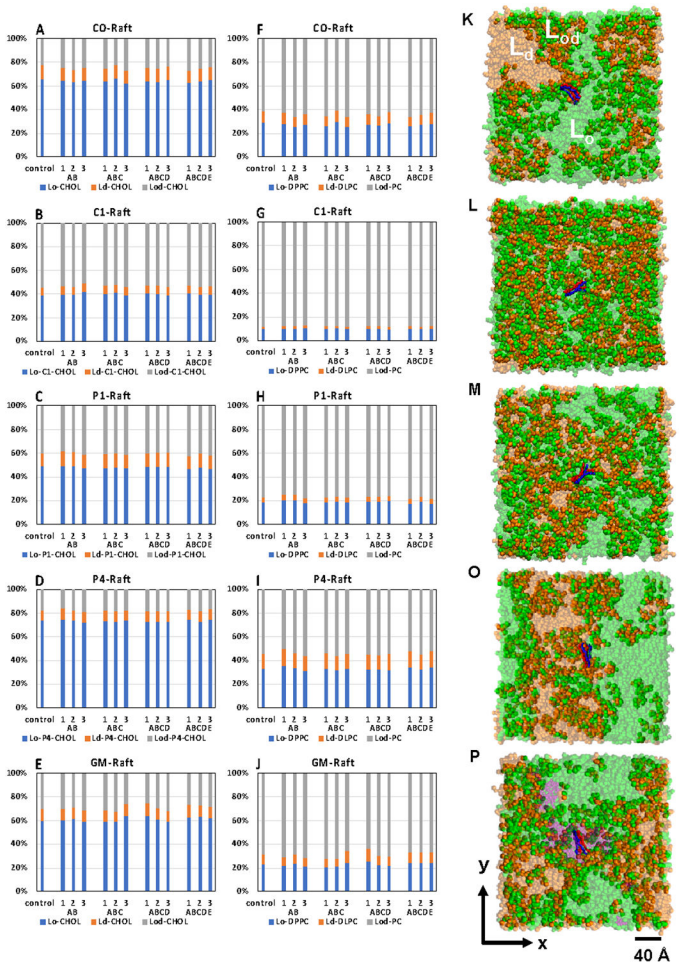

Figure 4.

Lipid composition (A-J) and lateral organization (K-P) of Lo, Ld and Lod domains in fibril/raft complexes. The percentages of cholesterol (A-E), DPPC and DLPC (F-J) in each lipid domain (Lo, Ld or Lod) are shown. Representative lateral views of membrane-bound dimer fibril (blue and red ribbons) in CO-raft (K), C1-raft (L), P1-raft (M), P4-raft (O) and GM-raft (P) are shown. DPPC-rich Lo in light green, DLPC-rich Ld in light orange, and mixed DPPC-DLPC Lod in dark green and dark orange are shown. GM1–1 is in light purple. A scale bar of 40 Å is given.

Author Manuscript Author Manuscript Author Manuscript Author Manuscript

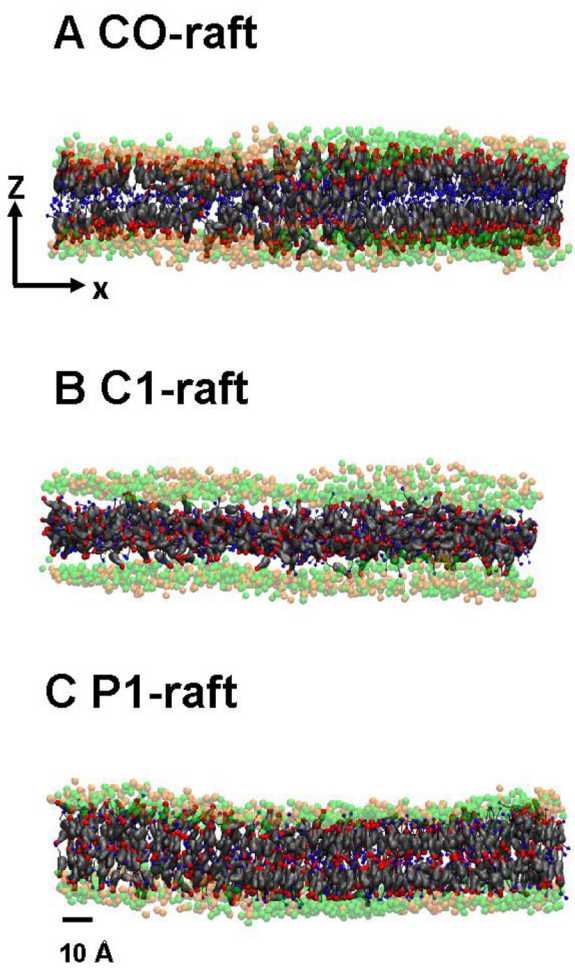

Figure 5.

Representative transverse views of PO4 headgroup of DPPC in green, DLPC in orange, and ROH headgroup in red and C2 tail group in blue of CHOL or modified CHOL for CO-raft (A), C1-raft (B) and P1-raft (C). A scale bar of 10 Å is given.

Author Manuscript Author Manuscript Author Manuscript Author Manuscript

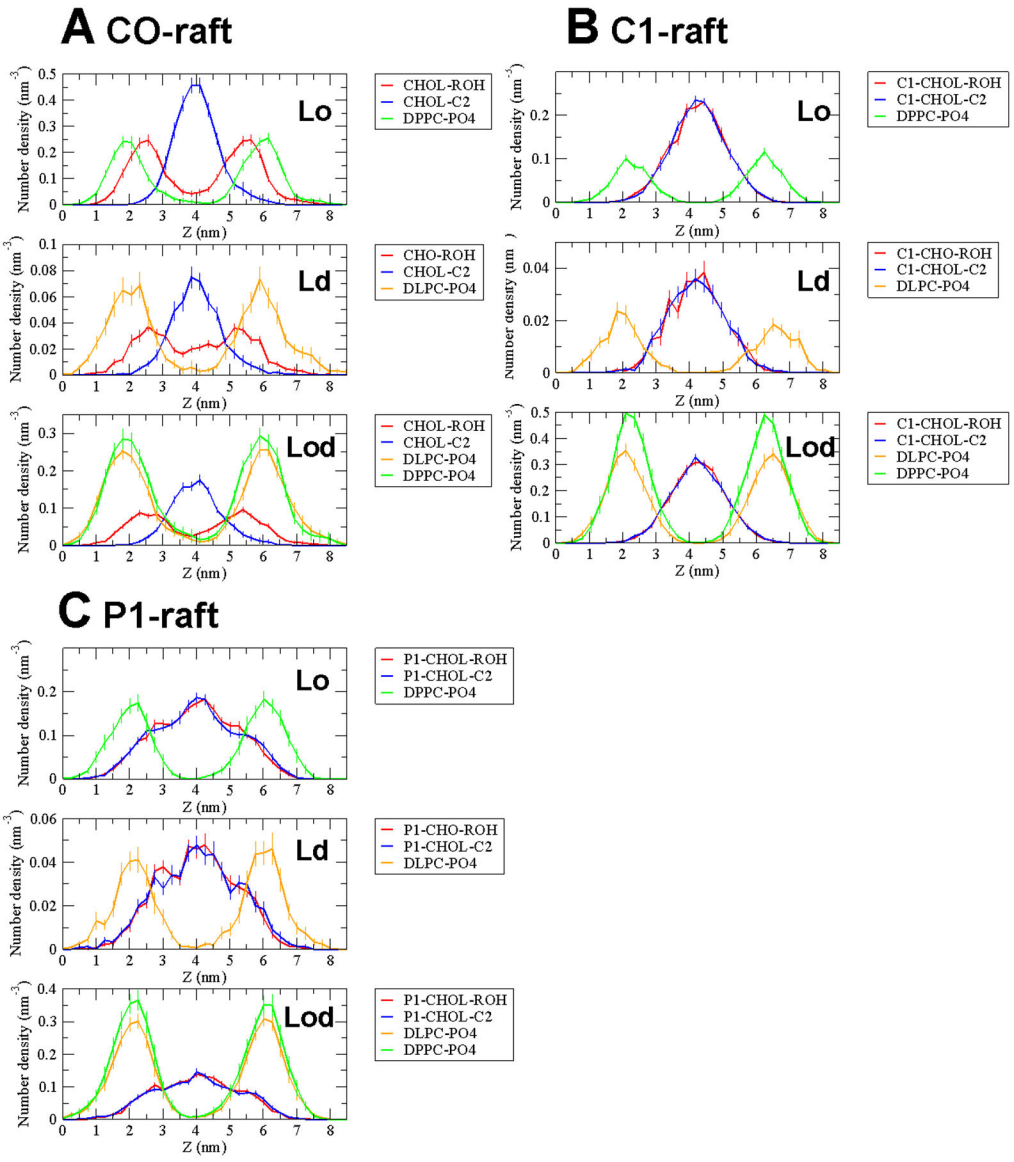

Figure 6.

Average number density profile of lipid groups in the Lo (upper panel), Ld (mid panel) and Lod (lower panel) for CO-raft (A), C1-raft (B) and P1-raft (C) over the last 5 μs of simulations.

Author Manuscript Author Manuscript Author Manuscript Author Manuscript

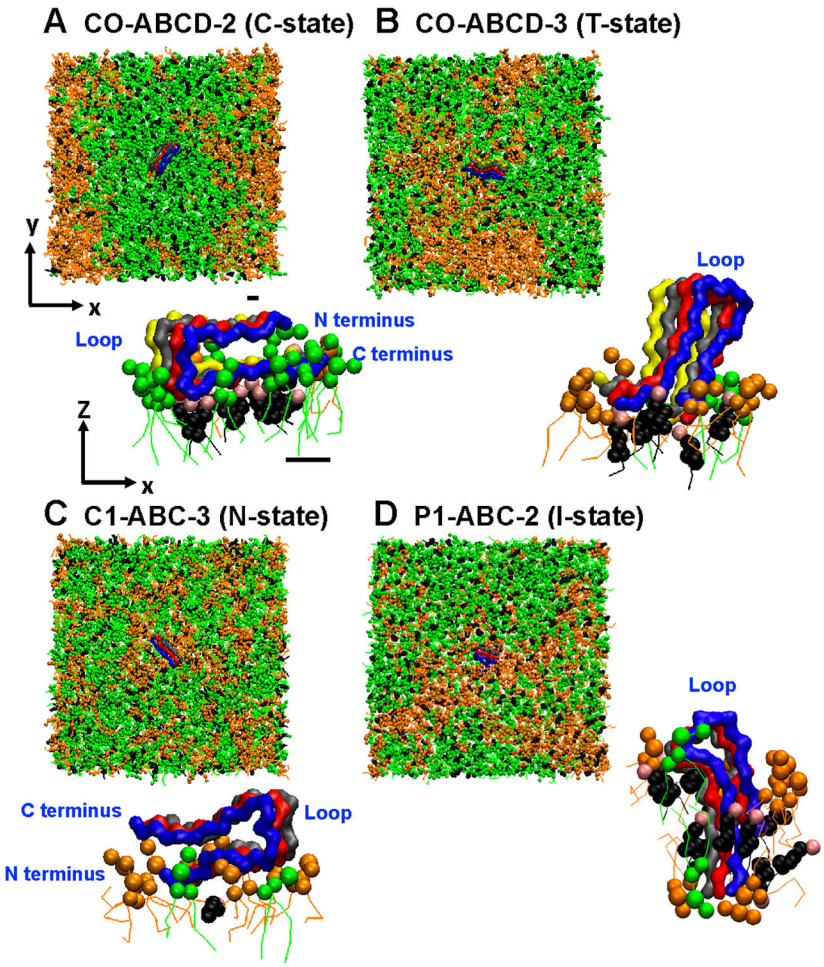

Figure 7.

Transverse (x, z) and lateral (x, y) views of CO-ABCD-2 in the C-state (A), CO-ABCD-3 in the T-state (B), C1-ABC-3 in the N-state (C), and P1-ABC-2 in the I-state (D) after 20 μs of simulations. The C-terminus, N-terminus and Loop regions of the fibrils are shown. Headgroups of DPPC, DLPC and cholesterol rings are in green, orange and black spheres, respectively. The lipids in the nearest (less than 5 Å between the atoms of the lipid and those of the protein) lipid shell surrounding the fibrils are shown. The CHO headgroup (ROH) is represented by a silver sphere. A scale bar of 10 Å is shown.

Author Manuscript Author Manuscript Author Manuscript Author Manuscript

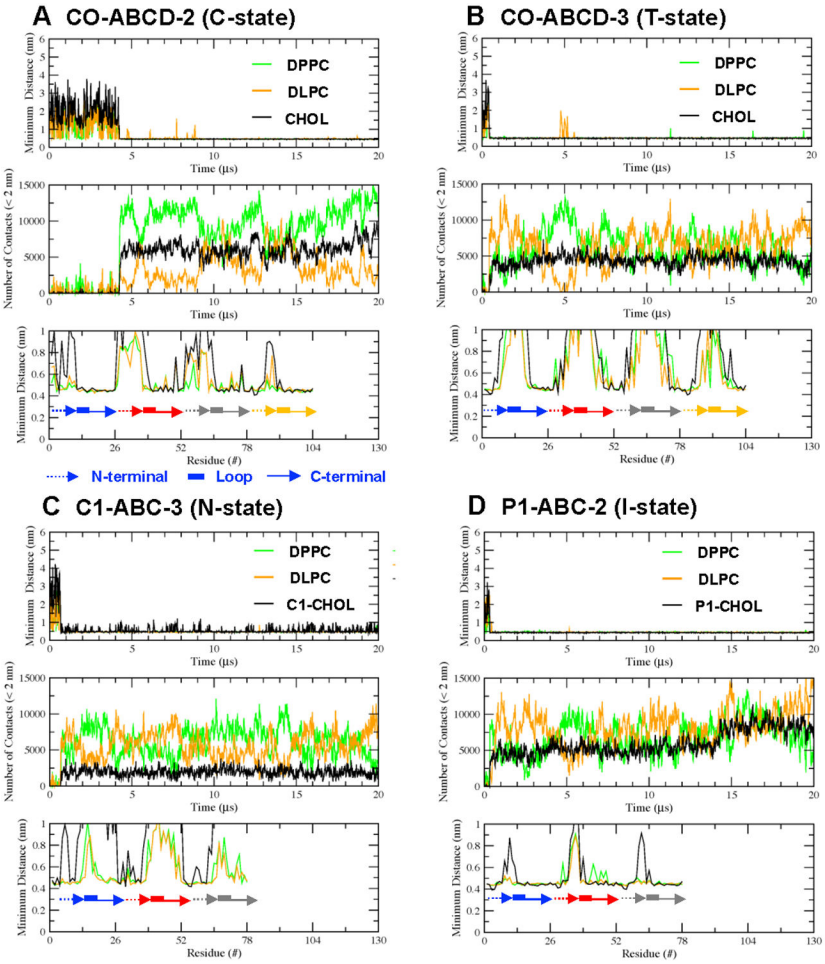

Figure 8.

Fibril/lipid binding kinetics analysis for CO-ABCD-2 in the C-state (A) and CO-ABCD-3 in the T-state (B), C1-ABC-3 in the N-state and P1-ABC-2 in the I-state. The three-panel plot shows the minimum distance between the lipid and protein atoms vs. time (upper panel), number of contacts between lipid and protein atoms that are less than 2 nm vs. time (mid panel), and the minimum distance averaged over the last 5 μs vs. residue location of the fibril (lower panel). The N-terminal (dashed arrow), Loop (solid line) and C-terminal (solid arrow) regions of each fibril chain (A in blue, B in red, C in gray, and D in yellow) are shown.

Author Manuscript Author Manuscript Author Manuscript Author Manuscript

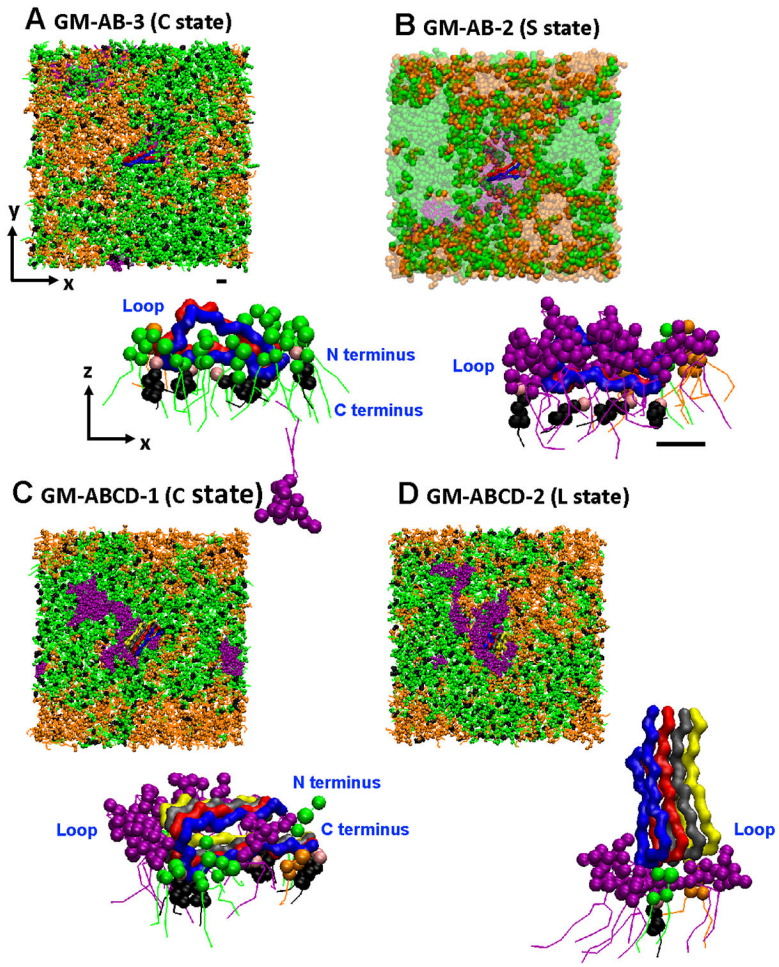

Figure 9.

Transverse (x, z) and lateral (x, y) views of GM-AB-3 in the C-state (A), GM-AB-2 in the S-state (B), GM-ABCD-1 in the C-state (C) and GM-ABCD-2 in the L-state (D). The Lo, Ld and Lod domains (B) were identified. GM1 lipids are shown in purple. See Fig. 7 legend for details.

Author Manuscript Author Manuscript Author Manuscript Author Manuscript

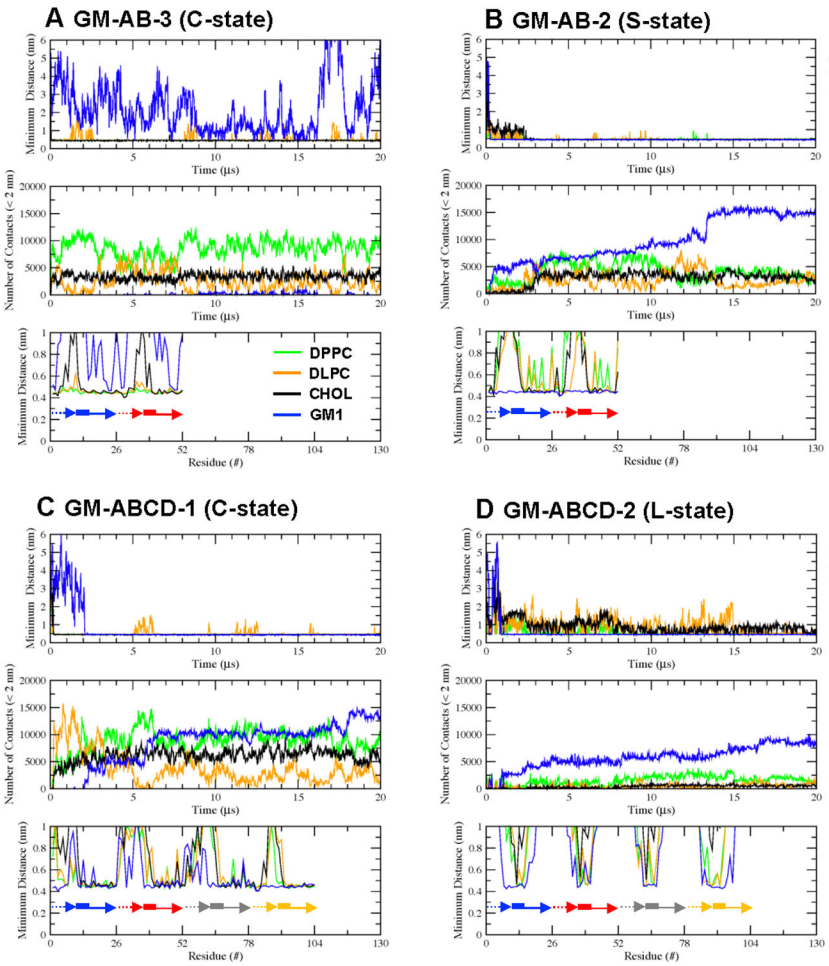

Figure 10.

Fibril/lipid binding kinetics analysis for GM-AB-3 in the C-state (A), GM-AB-2 in the S-state (B), GM-ABCD-1 in the C-state (C) and GM-ABCD-2 in the L-state (D). See Fig.8 legend for details.

Author Manuscript

Author Manuscript

Author Manuscript

Table 1.

Membrane-bound states of fibrils.

Raft	Chain number	Replicate 1	Replicate 2	Replicate 3
CO	2	AB-1 (C)	AB-2 (C)	AB-3 (C)
	3	ABC-1 (C)	ABC-2 (C)	ABC-3 (C)
	4	ABCD-1 (C)	ABCD-2 (C)	**ABCD-3 (T)**
	5	ABCDE-1 (C)	ABCDE-2 (C)	ABCDE-3 (C)
C1	2	AB-1 (C)	AB-2 (C)	AB-3 (C)
	3	**ABC-1 (T)**	ABC-2 (C)	**ABC-3 (N)**
	4	ABCD-1 (C)	ABCD-2 (C)	**ABCD-3 (T)**
	5	ABCDE-1 (C)	ABCDE-2 (C)	ABCDE-3 (C)
P1	2	AB-1 (C)	AB-2 (C)	AB-3 (C)
	3	ABC-1 (C)	**ABC-2 (I)**	ABC-3 (C)
	4	**ABCD-1 (N)**	ABCD-2 (C)	ABCD-3 (C)
	5	ABCDE-1 (C)	ABCDE-2 (C)	ABCDE-3 (C)
P4	2	AB-1 (C)	AB-2 (C)	AB-3 (C)
	3	ABC-1 (C)	ABC-2 (C)	ABC-3 (C)
	4	ABCD-1 (C)	**ABCD-2 (T)**	**ABCD-3 (T)**
	5	ABCDE-1 (C)	**ABCDE-2 (T)**	**ABCDE-3 (N)**
GM	2	**AB-1 (S)**	**AB-2 (S)**	AB-3 (C)
	3	**ABC-1 (N)**	**ABC-2 (N)**	ABC-3 (C)
	4	ABCD-1 (C)	**ABCD-2 (L)**	**ABCD-3 (N)**
	5	ABCDE-1 (C)	ABCDE-2 (C)	**ABCDE-3 (N)**

Membrane-bound states of fibrils in CO-, C1-, P1-, P4- and GM-rafts after 20 μs of MD simulations for different chain numbers, and from three simulation replicates (−1, −2 and −3). For clarity, the complexes exhibiting non-C states, i.e., T, N, I, S and L, are highlighted in bold.